Ca^{2+}-Calmodulin Dependent Inactivation of Cardiac Ryanodine Receptor is a Major Determinant of Ca^{2+} Alternans in Intact Hearts

Jinhong Wei[1,a], Jinjing Yao[1,b], Darrell Belke[1], Wenting Guo[1,c], Xiaowei Zhong[1,c], Bo Sun[1,b], Ruiwu Wang[1], John Paul Estillore[1], Alexander Vallmitjana[2], Raul Benitez[2,3], Leif Hove-Madsen[4,], Enrique Alvarez-Lacalle[5], Blas Echebarria[5], and S.R. Wayne Chen[1,d,*]

From the [1]Libin Cardiovascular Institute, Department of Physiology and Pharmacology, University of Calgary, Calgary, Alberta T2N 4N1, Canada, [2]Department of Automatic Control, Universitat Politècnica de Catalunya, 08034, Barcelona, Spain, [3]Institut de Recerca Sant Joan de Déu (IRSJD), 08950, Barcelona, Spain; [4]Biomedical Research Institute Barcelona IIBB-CSIC and IIB Sant Pau, Hospital de Sant Pau, 08025, Barcelona, Spain; and [5]Departament de Física, Universitat Politècnica de Catalunya-Barcelona Tech, Barcelona, Spain

Running Title: CaM Control of Ca^{2+} Alternans

[a]JW, recipient of the Libin Cardiovascular Institute and Cumming School of Medicine Postdoctoral Fellowship Award.
[b]JY, BS, recipients of the Alberta Innovates-Health Solutions (AIHS) Fellowship Award.
[c]XZ, WG, recipients of the Alberta Innovates-Health Solutions (AIHS) Studentship Award.

[d]SRWC, AIHS Scientist.

*To whom correspondence should be addressed. S.R. Wayne Chen, 3330 Hospital Drive N.W., Calgary, Alberta, Canada, T2N 4N1. Tel.: 403-220-4235; e-mail: swchen@ucalgary.ca; Blas Echebarria, blas.echebarria@upc.edu; Enrique Alvarez-Lacalle, enric.alvarez@upc.edu; or Leif Hove-Madsen, leif.hove@iibb.csic.es

Key words: Ventricular tachyarrhythmia, Ca^{2+} alternans, Ca^{2+} transient refractoriness, sarcoplasmic reticulum, cardiac ryanodine receptor, confocal Ca^{2+} imaging, intact heart imaging

ABSTRACT

Rationale: Ca^{2+} alternans plays an essential role in cardiac alternans that can lead to ventricular fibrillation, but the mechanism underlying Ca^{2+} alternans remains undefined. Increasing evidence suggests that Ca^{2+} alternans results from alternations in the inactivation of cardiac ryanodine receptor (RyR2). However, what inactivates RyR2 and how RyR2 inactivation leads to Ca^{2+} alternans are unknown.

Objective: To determine the role of calmodulin (CaM) on Ca^{2+} alternans in intact working mouse hearts.

Methods and Results: We used an *in vivo* local gene delivery approach to alter CaM function by directly injecting adenoviruses expressing CaM-wild type (CaM-WT), a loss-of-function CaM mutation, CaM (1-4), and a gain-of-function mutation, CaM-M37Q, into the anterior wall of the left ventricle of RyR2 WT or mutant mouse hearts. We monitored Ca^{2+} transients in ventricular myocytes near the adenovirus injection sites in Langendorff-perfused intact working hearts using confocal Ca^{2+} imaging. We found that CaM-WT and CaM-M37Q promoted Ca^{2+} alternans and prolonged Ca^{2+} transient recovery in intact RyR2 WT and mutant hearts, whereas, CaM (1-4) exerted opposite effects. Altered CaM function also affected the recovery from inactivation of the L-type Ca^{2+} current, but had no significant impact on sarcoplasmic reticulum Ca^{2+} content. Further, we developed a novel numerical myocyte model of Ca^{2+} alternans that incorporates Ca^{2+}-CaM-dependent regulation of RyR2 and the L-type Ca^{2+} channel. Remarkably, the new model recapitulates the impact on Ca^{2+} alternans of altered CaM and RyR2 functions under 9 different experimental conditions. Our simulations reveal that diastolic cytosolic Ca^{2+} elevation as a result of rapid pacing triggers Ca^{2+}-CaM dependent inactivation of RyR2. The resultant RyR2 inactivation diminishes SR Ca^{2+} release, which in turn reduces diastolic cytosolic Ca^{2+}, leading to alternations in diastolic cytosolic Ca^{2+}, RyR2 inactivation, and SR Ca^{2+} release (i.e. Ca^{2+} alternans).

Conclusions: Our results demonstrate that inactivation of RyR2 by Ca^{2+}-CaM is a major determinant of Ca^{2+} alternans, making Ca^{2+}-CaM dependent regulation of RyR2 an important therapeutic target for cardiac alternans.

INTRODUCTION

Cardiac alternans is a beat-to-beat alternation in the magnitude of a cardiac parameter such as the force of contraction (mechanical alternans), a component of the electrocardiogram (ECG) waveform (e.g. T-wave alternans), the action potential (AP) duration (APD alternans), or the amplitude of the cytosolic Ca^{2+} transient (Ca^{2+} alternans). Importantly, one or more types of these cardiac alternans are frequently observed in various experimental settings and in patients with ischemic heart disease and heart failure[1, 2]. Therefore, cardiac alternans is a well-recognized risk factor for ventricular fibrillation (VF) and sudden cardiac death (SCD) [2-6]. However, the molecular mechanisms underlying cardiac alternans remain incompletely understood.

Among different forms of cardiac alternans, Ca^{2+} alternans is thought to play a primary role in the genesis of cardiac alternans [7-12]. For instance, Ca^{2+} alternans could still be observed in cardiomyocytes that were voltage-clamped, suggesting that APD alternans is not required for Ca^{2+} alternans [8]. Furthermore, Wan et al [13] simultaneously recorded the membrane potential and Ca^{2+} transients in isolated cardiomyocytes, and showed that Ca^{2+} alternans occurred in the absence of APD alternans, whereas, APD alternans did not occur without Ca^{2+} alternans. An increased body of evidence supports the notion that Ca^{2+} dysregulation has a primary role in cardiac alternans [7-11, 13-17]. Therefore, understanding how Ca^{2+} alternans occurs is key to the understanding of cardiac alternans and the treatment of VF and SCD.

It is generally believed that Ca^{2+} alternans results from altered intracellular Ca^{2+} cycling [11, 18-21]. It is well established that the amplitude of the Ca^{2+} transient in cardiomyocytes as a result of Ca^{2+}-induced Ca^{2+} release depends on (i) the L-type Ca^{2+} current (I_{Ca}), (ii) the SR Ca^{2+} content, and (iii) the activity of RyR2 [18]. Studies have consistently shown that there are no beat-to-beat alternations in the peak I_{Ca} during Ca^{2+} alternans [17, 22, 23]. Further, beat-to-beat alternation in the peak I_{Ca}, when it was observed, was found to be a consequence rather than a cause of Ca^{2+} alternans [24, 25]. These observations suggest that alternation in the peak I_{Ca} is unlikely to be a primary cause of Ca^{2+} alternans. Similarly, since Ca^{2+} alternans was observed in the presence or absence of beat-to-beat alternations in SR Ca^{2+} content [9, 23], it is also unlikely that alternation in SR Ca^{2+} content is a primary cause of Ca^{2+} alternans. This leaves the activity of RyR2 as a pivotal candidate for the occurrence of Ca^{2+} alternans. Consistent with this view, pharmacological and experimental interventions and genetic manipulations that alter the activity of RyR2 markedly affect the propensity for Ca^{2+} alternans [22, 26-28].

It has been suggested that the refractoriness of RyR2 or the recovery of RyR2 from some kind of inactivation contributes to the induction of Ca^{2+} alternans [16, 23, 27, 29, 30]. In support of these experimental observations, numerical modeling studies have also shown the importance of RyR2 refractoriness in the induction of Ca^{2+} alternans [20, 31-33]. However, despite its fundamental significance, the molecular basis of RyR2 inactivation/refractoriness that contributes to Ca^{2+} alternans remains unknown.

During SR Ca^{2+} release, the released Ca^{2+} binds to CaM, and the Ca^{2+}-CaM complex inhibits RyR2 [34-36]. Hence, Ca^{2+}-CaM dependent inactivation of RyR2 follows each SR Ca^{2+} release. CaM also plays an important role in the termination of RyR2-mediated Ca^{2+} release [37]. Expression of CaM WT promotes the termination of Ca^{2+} release in HEK293 cells expressing RyR2, whereas, the Ca^{2+}-insensitive CaM mutation, CaM (1-4) that disables all 4 EF-hand Ca^{2+} binding motifs, suppresses the termination of Ca^{2+} release [37]. CaM has also been shown to affect the refractoriness of SR Ca^{2+} release [38]. Thus, by modulating the termination and refractoriness of SR Ca^{2+} release, CaM likely plays a key role in the relaxation of cardiac muscle. Notwithstanding its physiological significance, the role of CaM in the

induction of Ca^{2+} alternans is completely undefined.

In the present study, we assessed the role of CaM in the induction of Ca^{2+} alternans in intact working hearts. We performed laser-scan confocal Ca^{2+} imaging of cardiomyocytes in intact wild type (WT) and RyR2 mutant hearts infected *in vivo* with adenoviruses expressing CaM-WT or CaM mutants. We found that CaM-WT and a gain-of-function (GOF) CaM mutant (M37Q) promoted Ca^{2+} alternans and prolonged Ca^{2+} transient recovery, whereas, a loss-of-function (LOF) CaM mutation CaM (1-4) suppressed Ca^{2+} alternans and shortened Ca^{2+} transient recovery in both WT and RyR2 mutant hearts. Furthermore, we developed a novel numerical myocyte model for Ca^{2+} alternans, which incorporates the key feature of RyR2 inactivation by Ca^{2+}-CaM. Remarkably, our new model recapitulates the impact of RyR2 and CaM mutations on Ca^{2+} alternans. Our numerical simulations also reveal novel and important insights into the induction and progression of Ca^{2+} alternans.

METHODS

To assess the role of CaM in Ca^{2+} alternans in cardiac cells in the setting of intact working hearts and to avoid global detrimental impact of altered CaM function, we performed local adenovirus-mediated gene delivery *in vivo* by directly injecting adenoviruses expressing the CaM-WT, CaM (1-4), and CaM-M37Q mutants into the anterior wall of the left ventricle [39]. Five days after adenovirus injection the hearts were isolated and Ca^{2+} transients were measured in Langendorff-perfused intact hearts loaded with Rhod-2 AM using laser scanning confocal Ca^{2+} imaging as described previously[40, 41]. The recovery of voltage-induced Ca^{2+} transients was determined by using the S1S2 stimulation protocol as described previously with some modifications [16, 27, 28]. SR Ca^{2+} content was determined by measuring the amplitude of Ca^{2+} transients induced by local delivery of 20 mM caffeine. The recovery from inactivation of the L-type Ca^{2+} current was determined by using whole-cell patch-clamp recordings of isolated ventricular myocytes and the S1-S2 stimulation protocol as described previously [38, 42]. The levels of adenovirus-mediated expression of CaM-WT and CaM mutants were determined by immunoblotting. Numerical simulations were performed using a modification of the Bondarenko model of a mouse ventricular myocyte [43]. Adult RyR2-R4496C$^{+/-}$ and RyR2-E4872Q$^{+/-}$ heterozygous mutant and WT control mice (8-16 weeks) were used for all experiments. Detailed methods are provided in the Online Data Supplement.

RESULTS

CaM is an important determinant of Ca^{2+} alternans in intact hearts

To assess the role of CaM in Ca^{2+} alternans, we determined the effect of altered CaM function on Ca^{2+} alternans. We used two CaM mutations: a loss-of-function (LOF) CaM mutation, CaM (1-4) in which all 4 EF-hand Ca^{2+} binding sites are disabled, and a gain-of-function (GOF) CaM mutation, CaM-M37Q that enhances the CaM-dependent inhibition of RyR2-mediated spontaneous Ca^{2+} release [44]. To study Ca^{2+} alternans in the context of intact hearts and to minimize systemic adverse effect of CaM mutations, we infected mouse hearts *in vivo* by directly injecting adenoviruses harboring the CaM-WT, CaM (1-4) or CaM-M37Q mutant (Suppl. Fig. S1A) into the anterior wall of the left ventricle [39]. We monitored Ca^{2+} transients in ventricular myocytes near the adenovirus injection site in Langendorff-perfused intact hearts using confocal Ca^{2+} imaging. We also recorded Ca^{2+} transients in ventricular myocytes in the posterior wall of the left ventricle (away from the anterior injection site), which serves as an internal

control (Suppl. Fig. S1B). As shown in Fig. 1, Ca^{2+} alternans in intact hearts without adenovirus injection (control) occurred at a stimulation frequency of ~10-11 Hz (Fig. 1A, E). This threshold frequency at which alternans occurs was decreased to ~8-9 Hz in ventricular myocytes near the CaM-WT adenovirus injection site in the anterior wall of the left ventricle (Fig. 1B, E). The threshold frequency for Ca^{2+} alternans in ventricular myocytes near the CaM-M37Q injection site was substantially decreased to ~7 Hz (Fig. 1D, E). In contrast, the threshold frequency for Ca^{2+} alternans in ventricular myocytes near the CaM (1-4) injection site was markedly increased to ~12-13 Hz (Fig. 1C, E). On the other hand, there were no significant differences in the alternans ratios at 6-14 Hz in ventricular myocytes in the posterior wall of the left ventricle (away from the adenovirus injection site) with or without infection with CaM-WT, CaM (1-4) or CaM-M37Q adenoviruses (Suppl. Fig. S1C). Furthermore, immunoblotting analysis showed a significantly increased level of CaM expression after infection with CaM-WT, CaM (1-4) or CaM-M37Q adenoviruses in the anterior wall around the injection site, but an unchanged level of CaM expression in the posterior wall away from the injection site, compared to control (Suppl. Fig. S1F, G). Therefore, the adenovirus-injection mediated expression of CaM-WT, CaM-M37Q, and CaM (1-4) and their functional impact were confined to the area near the injection site.

To directly visualize the confined expression of locally injected CaM-WT or CaM mutant adenoviruses, we employed adenoviruses co-expressing CaM-WT or CaM (1-4) together with the green fluorescence protein (GFP) marker (Fig.2A). We performed the same local *in vivo* gene delivery to the mouse hearts by directly injecting adenoviruses expressing CaM-WT/GFP or CaM (1-4)/GFP into the anterior wall of the left ventricle. As shown in Fig.2, the fluorescent GFP marker was detected only in the anterior wall around the injection site, but not in the posterior wall away from the injection site, nor in the control heart (Fig.2B). We also carried out confocal Ca^{2+} imaging of intact hearts locally infected with or without the CaM-WT/GFP or CaM (1-4)/GFP adenoviruses to assess their impact on Ca^{2+} alternans (Fig.2C). As with CaM-WT and CaM (1-4) adenoviruses, we found that CaM-WT/GFP decreased the threshold frequency at which alternans occurs to ~8-9 Hz (from ~10-11 Hz in control), whereas, CaM (1-4)/GFP increased the alternans threshold frequency to ~12-13 Hz (Suppl. Fig.S2A-D). There were no significant differences in the alternans ratios at all stimulation frequencies (6-14 Hz) between CaM-WT and CaM-WT/GFP or between CaM (1-4) and CaM (1-4)/GFP adenovirus infected intact hearts (Suppl. Fig. S3A). Furthermore, expression of CaM-WT/GFP or CaM (1-4)/GFP did not significantly affect the amplitude, time-to-peak, or decay time (at 50% or 90%) of Ca^{2+} transients compared to control (Suppl. Fig.S4). Immunoblotting analysis also showed a significantly increased level of CaM expression after infection with CaM-WT/GFP or CaM (1-4)/GFP adenoviruses in the anterior wall around the injection site, but an unchanged level of CaM expression in the posterior wall away from the injection site compared to control (Fig. 2D, E). Taken together, these observations indicate that enhancing CaM function (as in the GOF CaM mutation M37Q) promotes Ca^{2+} alternans, whereas suppressed CaM function (as in the LOF CaM mutation CaM (1-4)) diminished it. Therefore, CaM is an important determinant of pacing-induced Ca^{2+} alternans in intact hearts.

CaM regulates the recovery of depolarization-induced Ca^{2+} transients in intact hearts

Ca^{2+} alternans is thought to result from beat-to-beat alternations in the refractoriness of depolarization-induced Ca^{2+} transients [16, 23, 27, 29, 30]. Thus, CaM may affect Ca^{2+} alternans by modulating Ca^{2+} transient refractoriness. To test this, we assessed the effect of CaM-WT, CaM (1-4), or CaM-M37Q on the recovery of depolarization-induced Ca^{2+} transients in intact hearts. The recovery of Ca^{2+} transients in ventricular myocytes near or away from the adenovirus injection sites was determined using the S1S2 stimulation protocol [16] in isolated Langendorff-perfused intact hearts. As shown in Fig.1, the recovery of

the Ca^{2+} transient amplitude at various S1S2 intervals (~60-160ms) was slightly (but not significantly) prolonged in ventricular myocytes near the CaM-WT adenovirus injection site in the anterior wall of the left ventricle (Fig. 1G, J, K), and was markedly prolonged in cells near the CaM-M37Q injection site (Fig. 1I, J, K), compared to that in ventricular myocytes without infection (control) (Fig. 1F, J, K). On the other hand, the recovery of the Ca^{2+} transient amplitude in ventricular myocytes near the CaM (1-4) adenovirus injection site was substantially accelerated (Fig. 1H, J, K). There are no significant differences in the recovery of the Ca^{2+} transient amplitudes in ventricular myocytes in the posterior wall of the left ventricle (away from the adenovirus injection site) with or without infection with CaM-WT, CaM (1-4) or CaM-M37Q adenoviruses (Suppl. Fig. S1D). Furthermore, the recovery of the Ca^{2+} transient amplitude at various S1S2 intervals (~75-125ms) was slightly and significantly prolonged in ventricular myocytes near the CaM-WT/GFP adenovirus injection site in the anterior wall of the left ventricle compared to that in ventricular myocytes without infection (control) (Suppl. Fig. S2E-I). In contrast, the recovery of the Ca^{2+} transient amplitude in ventricular myocytes near the CaM (1-4)/GFP adenovirus injection site was substantially accelerated compared to control (Suppl. Fig. S2E-I). There were no significant differences in the recovery of the Ca^{2+} transient amplitude at all S1S2 intervals (~50-200 ms) between CaM-WT and CaM-WT/GFP or between CaM (1-4) and CaM (1-4)/GFP adenovirus infected intact hearts (Suppl. Fig. S3B). Collectively, these observations indicate that the GOF CaM-M37Q mutation prolongs the recovery of Ca^{2+} transients, whereas the LOF CaM (1-4) mutation shortens it. Thus, CaM has an important role in determining the recovery of Ca^{2+} transients.

Effects of CaM-WT and the CaM (1-4) mutant on SR Ca^{2+} content and the recovery from inactivation of the L-type Ca^{2+} current

SR Ca^{2+} content is one of the key determinants of Ca^{2+} transient amplitude. To assess whether the effects of altered CaM function on Ca^{2+} transient alternans are secondary to CaM-dependent changes in SR Ca^{2+} content, we measured SR Ca^{2+} content in GFP-expressing ventricular myocytes isolated from tissues near the CaM-WT/GFP or CaM (1-4)/GFP adenovirus injection site in the anterior wall of the left ventricle. Single cell Ca^{2+} imaging showed that CaM WT/GFP- and CaM (1-4)/GFP-expressing ventricular myocytes displayed amplitude of caffeine (20 mM) induced Ca^{2+} release similar to that of control cells (Fig. 3A-D). Note that the level of fluorescence signals evoked by 20 mM caffeine was not saturated as a much higher level of fluorescence signals could still be detected under the same conditions [28]. Thus, adenovirus-mediated expression of CaM-WT or CaM (1-4) does not significantly alter the SR Ca^{2+} content in ventricular myocytes under our experimental conditions.

In ventricular myocytes, the L-type Ca^{2+} current triggers Ca^{2+} transients. Thus, it is possible that the recovery from inactivation of the L-type Ca^{2+} current would affect the recovery of Ca^{2+} transients. To test this possibility, we assessed and compared the recovery of the Ca^{2+} transient amplitude and the recovery from inactivation of the L-type Ca^{2+} current in isolated CaM WT/GFP- and CaM (1-4)/GFP-expressing ventricular myocytes and control cells using confocal Ca^{2+} imaging and whole cell patch-clamp recordings, respectively. CaM-WT significantly prolonged the recovery of the Ca^{2+} transient amplitude with an average 50% recovery time of ~270 ms, compared to control (~220 ms). In contrast, CaM (1-4) significantly accelerated the recovery of the Ca^{2+} transient amplitude with an average 50% recovery time of ~140 ms (Fig. 3E-I). As with the recovery of the Ca^{2+} transient amplitude, CaM-WT significantly prolonged the recovery from inactivation of the L-type Ca^{2+} current with an average 50% recovery time of ~85ms compared to control (~60 ms), whereas CaM (1-4) significantly accelerated it with an average 50% recovery time of ~40 ms (Fig. 3J-N). However, the 50% recovery time from inactivation of the L-type Ca^{2+} current is markedly shorter than the 50% recovery time of the Ca^{2+} transient amplitude in the control, CaM-WT or CaM (1-4) expressing cells, respectively. In other words,

there is little or no recovery of Ca^{2+} transients from inactivation when the L-type Ca^{2+} current has already recovered to 50%. This implies that although the recovery from inactivation of the L-type Ca^{2+} current can influence the recovery of Ca^{2+} transient amplitude, it is unlikely to be the rate-limiting factor. Furthermore, CaM WT or mutant did not significantly alter the peak L-type Ca^{2+} current (I_{Ca}) (Suppl. Fig. S3D), similar to those reported previously [38, 45]. These observations suggest that other factors, for instance, the recovery from inactivation of the RyR2 channel may play a critical role in determining the recovery of the Ca^{2+} transient amplitude. Consistent with this view, experimental and numerical modeling studies also suggest that the recovery of RyR2 from inactivation significantly contributes to the induction of Ca^{2+} transient alternans [16, 23, 27, 29, 30], [20, 33].

Effects of CaM mutations on Ca^{2+} alternans and Ca^{2+} transient recovery in intact RyR2-E4872Q hearts

We have previously shown that the RyR2-E4872Q mutation abolishes luminal Ca^{2+} activation of RyR2 and markedly promotes Ca^{2+} alternans [27, 28]. Thus, both CaM- and luminal Ca^{2+}-dependent regulation of RyR2 play an important role in Ca^{2+} alternans. To determine whether there is a cross-talk between the CaM- and luminal Ca^{2+}-dependent regulatory mechanisms of Ca^{2+} alternans, we assessed the effect of altered CaM function on Ca^{2+} alternans in intact RyR2-E4872Q mutant hearts. As shown in Fig.4, Ca^{2+} alternans in intact RyR2-E4872Q mutant hearts without injection (control) occurred at a stimulation frequency of ~8 Hz (Fig. 4A, D), which is significantly lower than that (~11 Hz) in intact WT hearts (Fig. 1). As with WT hearts, CaM (1-4) increased the threshold frequency for Ca^{2+} alternans from ~8 Hz to ~10 Hz in ventricular myocytes near the injection site in the anterior wall of the left ventricle of the RyR2-E4872Q hearts (Fig. 4B, D), whereas, CaM-M37Q decreased the threshold frequency for Ca^{2+} alternans from ~8 to ~5-6 Hz (Fig. 4C, D). On the other hand, there are no significant differences in alternans ratios at 5-12 Hz in ventricular myocytes in the posterior wall of the left ventricle (away from the injection site) of intact RyR2-E4872Q hearts with or without infection with CaM (1-4) or CaM-M37Q (Suppl. Fig. S5A).

We also assessed the effect of altered CaM function on the recovery of Ca^{2+} transients in intact RyR2-E4872Q mutant hearts. CaM (1-4) accelerated the recovery of depolarization-induced Ca^{2+} transient amplitude (Fig. 4F, H, I), whereas CaM-M37Q delayed the recovery of the Ca^{2+} transient amplitude in intact RyR2-E4872Q mutant hearts (Fig. 4G, H, I), compared to control (Fig. 4E, H, I). There are no significant differences in the recovery of the Ca^{2+} transient amplitude in ventricular myocytes in the posterior wall of the left ventricle (away from the adenovirus injection site) (Suppl. Fig. S5B, C). Thus, CaM can still modulate the Ca^{2+} transient recovery and Ca^{2+} alternans in intact RyR2-E4872Q hearts with diminished luminal Ca^{2+} regulation of RyR2.

Effects of CaM mutations on Ca^{2+} alternans and Ca^{2+} transient recovery in intact RyR2-R4496C hearts

We have also shown previously that the RyR2-R4496C mutation enhances luminal Ca^{2+} activation of RyR2 and dramatically suppresses Ca^{2+} alternans [28]. To further investigate the cross-talk between the CaM- and luminal Ca^{2+}-dependent regulatory mechanisms of Ca^{2+} alternans, we assessed the effect of altered CaM function on Ca^{2+} alternans in intact RyR2-R4496C mutant hearts. As shown in Fig.5, Ca^{2+} alternans in intact RyR2-R4496C hearts without injection occurred at a stimulation frequency of ~13-14 Hz (Fig. 5A, D), which is significantly higher than that (~11 Hz) in intact WT hearts (Fig. 1). CaM (1-4) increased the threshold frequency for Ca^{2+} alternans from ~13-14 to ~15 Hz in ventricular myocytes near the injection site in the anterior wall of the left ventricle of the RyR2-R4496C hearts (Fig. 5B, D),

whereas CaM-M37Q decreased the threshold frequency for Ca^{2+} alternans from ~13-14 to ~8-9 Hz (Fig. 5C, D). Similarly, there are no significant differences in alternans ratios at 8-15 Hz in ventricular myocytes in the posterior wall of the left ventricle (away from the injection site) of intact RyR2-R4496C hearts with or without infection with CaM (1-4) or CaM-M37Q (Suppl. Fig. S5D).

CaM (1-4) also accelerated the recovery of the Ca^{2+} transient amplitude (Fig. 5F, H, I), whereas CaM-M37Q delayed the recovery of the Ca^{2+} transient amplitude in intact RyR2-R4496C mutant hearts (Fig. 5G, H, I), compared to control (Fig. 5E, H, I). There are no significant differences in the recovery of the Ca^{2+} transient amplitude in ventricular myocytes in the posterior wall of the left ventricle (away from the injection site) of intact RyR2-R4496C hearts with or without infection with CaM (1-4) or CaM-M37Q (Suppl. Fig. S5E, F). Taken together, enhanced CaM function promotes, whereas, decreased CaM function suppresses Ca^{2+} alternans. In contrast, enhanced RyR2 luminal Ca^{2+} activation suppresses, whereas, decreased RyR2 luminal Ca^{2+} activation promotes Ca^{2+} alternans. Thus, CaM and RyR2 luminal Ca^{2+} activation regulate Ca^{2+} transient recovery and Ca^{2+} alternans in a counter-balanced manner.

A novel numerical model recapitulates the action of CaM in Ca^{2+} alternans in intact WT hearts

Previous numerical simulations have shown that RyR2 inactivation plays a key role in the induction of Ca^{2+} alternans [20, 33]. However, the molecular basis for RyR2 inactivation and the induction of Ca^{2+} alternans is unknown. Given the involvement of CaM in the inactivation of RyR2, the termination and refractoriness of Ca^{2+} release [34, 37, 38], and Ca^{2+} alternans (Figs. 1-5), we developed a numerical model of Ca^{2+} alternans by incorporating the Ca^{2+}-CaM dependent inactivation of RyR2 and recovery of RyR2 from this inactivation into the Bondarenko model of mouse ventricular myocytes [43] (Fig. 6A, B; Suppl. Fig. S6). The L-type Ca^{2+} channel (LTCC) is also known to be modulated by CaM [46]. Hence, we incorporated the Ca^{2+}-CaM dependent regulation of LTCC as well. Furthermore, since SR luminal Ca^{2+} activation of RyR2 is important for the induction of Ca^{2+} alternans [27, 28], we also included the highly steep activation of RyR2 by SR luminal Ca^{2+} into the modified model (Fig. 6A, B; Suppl. Fig. S6). In addition, we modified the binding of Ca^{2+} to CaM, added the Rhod-2 dye, and included mitochondria Ca^{2+} handling in the model. Remarkably, this new model recapitulates the induction and progression of pacing-induced Ca^{2+} alternans in intact WT hearts (Fig. 6C). The alternans ratios in RyR2-WT hearts at different pacing frequencies predicted by the model matched very closely those observed experimentally (Fig. 6C, G).

To model the impact of altered CaM function on Ca^{2+} alternans, we modified the level and/or the affinity of Ca^{2+} binding to CaM to simulate the functional impact of CaM-WT, CaM (1-4), and CaM-M37Q (Suppl. Materials). Importantly, our model also reproduced the effects of CaM-WT (Fig. 6D), CaM (1-4) (Fig. 6E), and CaM-M37Q (Fig. 6F) on Ca^{2+} alternans at different pacing frequencies in intact RyR2 WT hearts (Fig. 6G). Therefore, our numerical model recapitulates not only the induction and progression of pacing-induced Ca^{2+} alternans in intact hearts, but also the impact of CaM WT and mutants on Ca^{2+} alternans.

Numerical simulation reproduces the effects of RyR2 and CaM mutations on Ca^{2+} alternans in intact RyR2-E4872Q and RyR2-R4496C mutant hearts

The RyR2-E4872Q mutation diminishes luminal Ca^{2+} activation and suppresses cytosolic Ca^{2+} activation of single RyR2 channels. E4872Q also increases the LTCC current to maintain the amplitude of Ca^{2+} transients as a compensatory response to reduced SR Ca^{2+} release [47]. On the other hand, the RyR2-

R4496C mutation enhances the luminal Ca^{2+} activation, but has little effect on the cytosolic Ca^{2+} activation of single RyR2 channels [48]. To determine whether our numerical model is also able to reproduce the effect of altered RyR2 function on Ca^{2+} alternans, we modified in the model the response of RyR2 to cytosolic and luminal Ca^{2+} activation to incorporate the functional impact of the RyR2-E4872Q or RyR2- R4496C mutation. As shown in Fig. 7, the alternans ratios at different pacing frequencies predicted by the model are remarkably similar to those obtained experimentally (Fig. 7A, E, D, H). More importantly, the model also recapitulated the actions of CaM (1-4) and CaM-M37Q mutations in Ca^{2+} alternans in the RyR2-E4872Q (Fig. 7B, C, D) and RyR2-R4496C (Fig. 7F, G, H) mutant hearts without implanting additional modifications to the model. Thus, the model is able to reproduce not only the effect of altered CaM function, but also the effect of altered RyR2 function on Ca^{2+} alternans in intact hearts. Taken together, our numerical model recapitulates the induction and progression of Ca^{2+} alternans in intact hearts under 9 different experimental conditions.

CaM is critical for RyR2 inactivation and Ca^{2+} alternans

We next used the newly developed, experimentally validated numerical model to explore the mechanism of Ca^{2+} alternans. We first assessed the role of CaM in the inactivation of RyR2 and the occurrence of Ca^{2+} alternans. We analyzed the fraction of inactivated RyR2 and cytosolic Ca^{2+} transients at a stimulation frequency of 12 Hz before and after removing CaM (i.e. setting the concentration of CaM to 0). As shown in Suppl. Fig. S7, removal of CaM from the system completely abolished RyR2 inactivation and Ca^{2+} alternans (Suppl. Fig.S7A, B). Thus, consistent with previous studies [20, 33], RyR2 inactivation and more specifically, Ca^{2+}-CaM-dependent RyR2 inactivation is a critical determinant of Ca^{2+} alternans.

Pacing-induced diastolic cytosolic Ca^{2+} elevation triggers Ca^{2+}-CaM dependent RyR2 inactivation and provokes diastolic cytosolic Ca^{2+} and RyR2 inactivation alternations

What then triggers Ca^{2+}-CaM-dependent inactivation of RyR2 and how does Ca^{2+}-CaM dependent RyR2 inactivation lead to Ca^{2+} alternans? To address these questions, we simulated the induction and progression of pacing-induced Ca^{2+} alternans using a S1S2 stimulation protocol with a basal stimulation (S1) at a given frequency (e.g. at the alternans threshold frequency, 10.6 Hz, as described in Supplemental Materials) followed by a second stimulation (S2) at various frequencies (e.g. 12 Hz) (Fig. 8A). We analyzed the levels of diastolic cytosolic Ca^{2+} and diastolic fraction of Ca^{2+}-CaM inactivated RyR2 in the steady state at various S2 stimulation frequencies (9-12 Hz) after switching from 10.6 Hz (S1) (Fig. 8B-D). We focused on the diastolic fraction of inactivated RyR2 because it determines the diastolic fraction of RyR2 available for activation and thus the magnitude of RyR2 mediated Ca^{2+} release and Ca^{2+} transients. As shown in Fig. 8C, the diastolic cytosolic Ca^{2+} progressively increased when the S2 stimulation frequency increased from 9 to 10.6 Hz (i.e. below the threshold frequency for Ca^{2+} alternans). Given the strict Ca^{2+} dependence of CaM dependent inactivation of RyR2, the diastolic fraction of Ca^{2+}-CaM inactivated RyR2 is expected to increase as a result of increasing diastolic cytosolic Ca^{2+}. That was indeed the case (Fig. 8D). Thus, pacing-induced elevation in diastolic cytosolic Ca^{2+} likely triggers Ca^{2+}-CaM dependent inactivation of RyR2.

Interestingly, when the S2 stimulation frequency increased to >10.6 Hz (i.e. above the alternans threshold frequency), the diastolic cytosolic Ca^{2+} progressively increased at one beat but decreased in the following beat (Fig. 8C, beats 29 and 30). Such a beat-to-beat alternation leads to a bifurcation in the diastolic cytosolic Ca^{2+} (increase at odd beats and decrease at even beats) (Fig. 8A). Similarly, we observed beat-to-beat alternation in the diastolic fraction of inactivated RyR2 (Fig. 8D). When the

pacing frequency is above the alternans threshold frequency (10.6 Hz), the diastolic fraction of inactivated RyR2 started to bifurcate (Fig. 8D, beats 29 and 30), corresponding to the bifurcation in the diastolic cytosolic Ca^{2+}. Thus, these simulations suggest that diastolic cytosolic Ca^{2+} alternations play a key role in diastolic RyR2 inactivation alternations that drive Ca^{2+} alternans.

Diastolic cytosolic Ca^{2+} alternation results from Ca^{2+} influx-efflux imbalance

To further explore why the diastolic cytosolic Ca^{2+} displayed beat-to-beat alternations when the stimulation frequency exceeds the alternans threshold frequency, we analyzed the major Ca^{2+} fluxes that contribute to the homeostasis of cytosolic Ca^{2+} at different pacing frequencies (Fig. 8E-G). These analyses revealed that the removal of Ca^{2+} out of the cytosol ($Ca^{2+}_{cyto}OUT=J_{uptake}+J_{NCX}$) and the influx of Ca^{2+} into the cytosol ($Ca^{2+}_{cyto}IN=J_{release}+J_{CaL}$) are identical at pacing frequencies below the alternans threshold frequency (<10.6Hz). However, at the pacing frequencies above the alternans threshold frequency (>10.6Hz), the removal of Ca^{2+} out of the cytosol ($Ca^{2+}_{cyto}OUT$) is smaller than the influx of Ca^{2+} into the cytosol ($Ca^{2+}_{cyto}IN$) at one beat (beat 29, Fig. 8 E-G). This imbalance leads to an elevation in diastolic cytosolic Ca^{2+} and the diastolic fraction of inactivated RyR2 (Fig. 8C, D, beat 29). In the next beat (beat 30), the situation is reversed; the removal of Ca^{2+} out of the cytosol is greater than the influx of Ca^{2+} into the cytosol at pacing frequencies above the alternans threshold frequency (>10.6 Hz) (Fig. 8E-G, beat 30), leading to a reduction in diastolic cytosolic Ca^{2+} and the diastolic fraction of inactivated RyR2 (Fig. 8C, D, beat 30). Thus, the imbalance between Ca^{2+} removal from and Ca^{2+} influx into the cytosol causes beat-to-beat alternations in diastolic cytosolic Ca^{2+}, in the diastolic fraction of inactivated RyR2, and thus in RyR2-mediated Ca^{2+} release and in Ca^{2+} transients.

We also analyzed the cytosolic Ca^{2+} transients and the fraction of inactivated RyR2 using stimulation frequencies (S1=7.6 Hz, S2=7.6-9 Hz) below the alternans threshold frequency (<10.6Hz) (Fig. 8H-N). After the system has stabilized (e.g. beats 29 and 30), there are no beat-to-beat alternations in diastolic cytosolic Ca^{2+} or in the diastolic fraction of inactivated RyR2 (Fig. 8J, K). All Ca^{2+} fluxes are balanced in the steady state (Fig. 8L-N, beats 29 and 30). Thus, there is no Ca^{2+} alternans when pacing frequency is below the alternans threshold frequency (10.6 Hz), despite the increase in the diastolic cytosolic Ca^{2+} and diastolic fraction of inactivated RyR2 with increasing pacing frequency.

Ca^{2+}-CaM dependent RyR2 inactivation drives Ca^{2+} flux imbalance

We next explored what triggers the imbalance of Ca^{2+} fluxes and diastolic cytosolic Ca^{2+} alternation. In cardiomyocytes, the level of diastolic cytosolic Ca^{2+} is largely determined by the L-type Ca^{2+} channel mediated Ca^{2+} influx (J_{CaL}), RyR2 mediated Ca^{2+} release ($J_{release}$), SR Ca^{2+} uptake (J_{uptake}), and Na^{+}/Ca^{2+} exchanger mediated Ca^{2+} removal (J_{NCX}). Rapid pacing induces changes in each of these currents (Fig. 8E, F, L, M). Since Ca^{2+} cycling in mouse cardiomyocytes is mainly determined by $J_{release}$ and J_{uptake}, the diastolic cytosolic Ca^{2+} level would be largely determined by $J_{release}$ and J_{uptake}. Moreover, J_{uptake} remains relatively linear in response to increasing pacing frequencies (Fig. 8E, L). Hence, rapid pacing-induced Ca^{2+} flux imbalance primarily results from the non-linear changes in $J_{release}$ (Fig. 8E, G), which is caused by Ca^{2+}-CaM dependent inactivation of RyR2. Therefore, Ca^{2+}-CaM dependent RyR2 inactivation by affecting $J_{release}$ drives Ca^{2+} flux imbalance, diastolic cytosolic Ca^{2+} alternation and thus Ca^{2+} alternans.

DISCUSSION

Experimental and mathematical modeling studies have suggested that beat-to-beat alternations in the inactivation/refractoriness of RyR2 plays an important role in cardiac Ca^{2+} alternans [20, 33]. However, the molecular mechanism underlying RyR2 inactivation/refractoriness remains largely unknown. CaM is known to inhibit RyR2 and promotes termination of RyR2-mediated Ca^{2+} release. CaM also modulates the refractoriness of RyR2-mediated Ca^{2+} release [34, 37, 38, 44]. Therefore, by virtue of its actions on RyR2 inactivation and Ca^{2+} release refractoriness, CaM would play a critical role in Ca^{2+} alternans. To directly test this idea, in the present study, we altered the function of CaM in cardiomyocytes in intact working hearts using adenovirus-mediated gene delivery of CaM mutants *in vivo* and assessed the impact of CaM mutations on Ca^{2+} transients using *in situ* intact heart Ca^{2+} imaging. We found that diminishing CaM function (as in CaM (1-4) mutation) shortened the recovery of Ca^{2+} transients and protected against Ca^{2+} alternans. In contrast, enhancing CaM function (as in CaM-M37Q mutation) prolonged the recovery of Ca^{2+} transients and promoted Ca^{2+} alternans. These data demonstrate, for the first time, that CaM is an important determinant of Ca^{2+} alternans in intact hearts.

We have demonstrated previously that activation of RyR2 by SR luminal Ca^{2+} plays an important role in Ca^{2+} alternans [27, 28]. Inhibiting RyR2 luminal Ca^{2+} activation promotes Ca^{2+} alternans, whereas enhancing RyR2 luminal Ca^{2+} activation suppresses Ca^{2+} alternans. These effects of altered RyR2 luminal Ca^{2+} regulation on Ca^{2+} alternans are opposite to those of altered CaM function. Hence, Ca^{2+} alternans is likely to be modulated by multiple competing regulators of RyR2, including CaM, luminal Ca^{2+}, and cytosolic Ca^{2+}. To understand this complex interplay, we developed a novel numerical myocyte model that incorporates RyR2 inactivation by Ca^{2+}-CaM as well as RyR2 activation by cytosolic and luminal Ca^{2+} a in a 4-state model of RyR2 [49]. Recently, high resolution three-dimensional structures of the CaM-RyR2 complexes in the absence and presence of Ca^{2+} have been resolved [36]. These structural analyses indicate that inactivation of RyR2 by CaM requires Ca^{2+} binding to CaM and the binding of the Ca^{2+}-CaM complex to RyR2, and that recovery of RyR2 from Ca^{2+}-CaM dependent inactivation requires the dissociation of Ca^{2+}-CaM from RyR2. To model this Ca^{2+}-dependent CaM inactivation of RyR2 and its recovery from inactivation, we included an inactivation rate proportional to the concentration of Ca^{2+}-CaM, while the recovery rate is assumed to be constant. For RyR2 activation, we assumed cytosolic Ca^{2+} activation is proportional to the square of the cytosolic Ca^{2+} concentration. Given the steep dependence of RyR2 activation by luminal Ca^{2+}, we modeled luminal Ca^{2+} activation of RyR2 with a large Hill coefficient (n = 6). Remarkably, our newly developed model recapitulates not only the impact of altered CaM function but also the impact of altered luminal Ca^{2+} activation of RyR2 on Ca^{2+} alternans under 9 different experimental conditions. This excellent match between experimental and simulation data indicates that Ca^{2+} alternans is largely controlled by the activity of RyR2 and is thus subjected to modulation by RyR2 regulators (cytosolic Ca^{2+}, luminal Ca^{2+}, and CaM).

Although it is well recognized that RyR2 inactivation underlies Ca^{2+} alternans, how RyR2 inactivation induces Ca^{2+} alternans remains largely undefined. Our simulation analyses reveal that the fraction of RyR2 available for stimulated SR Ca^{2+} release is determined by the diastolic fraction of Ca^{2+}-CaM inactivated RyR2, which is in turn determined by the diastolic cytosolic Ca^{2+} level (i.e. the level of cytosolic Ca^{2+} just before stimulation). The level of this diastolic cytosolic Ca^{2+} is largely determined by the net balance of SR Ca^{2+} release ($J_{release}$) and SR Ca^{2+} uptake (J_{uptake}). Increasing the pacing frequency (i.e. shortened cycle length) will reduce SR Ca^{2+} uptake, as the SR Ca^{2+} pump has less time to remove cytosolic Ca^{2+}. Reduced SR Ca^{2+} uptake will result in an elevation in diastolic cytosolic Ca^{2+}. On the other hand, this pacing-induced elevation in diastolic cytosolic Ca^{2+} will increase the level of the Ca^{2+}-CaM complex and the fraction of Ca^{2+}-CaM inactivated RyR2, which will reduce the fraction of RyR2 available for activation and thus SR Ca^{2+} release. Reduced SR Ca^{2+} release will in turn decrease diastolic cytosolic Ca^{2+}. Thus, increasing the pacing frequency has two opposing effects on the diastolic cytosolic

Ca^{2+} level. It is the net effect of these two opposing forces that determines the induction of Ca^{2+} alternans. When the pacing frequency is below the alternans threshold frequency, SR Ca^{2+} uptake equals to SR Ca^{2+} release at the steady state (Fig. 8). As such, there are no beat-to-beat alternations in the diastolic cytosolic Ca^{2+}, in RyR2 inactivation, or in RyR2-mediated Ca^{2+} release (i.e. no Ca^{2+} alternans). However, when the pacing frequency exceeds the alternans threshold, SR Ca^{2+} uptake is greater than SR Ca^{2+} release at one beat due to strong inactivation of RyR2 by the elevated diastolic cytosolic Ca^{2+}. This will result in a decrease in the diastolic cytosolic Ca^{2+}. The reduction in diastolic cytosolic Ca^{2+} will reduce the Ca^{2+}-CaM complex and thus the Ca^{2+}-CaM dependent RyR2 inactivation. This reduced RyR2 inactivation will increase SR Ca^{2+} release and diastolic cytosolic Ca^{2+} on the next beat. Thus, increasing pacing frequency above the alternans threshold leads to imbalance of SR Ca^{2+} uptake and Ca^{2+} release, causing beat-to-beat alternations in diastolic cytosolic Ca^{2+}, in RyR2 inactivation, and in RyR2-mediated Ca^{2+} release (i.e. Ca^{2+} alternans). Taken together, we propose that rapid pacing-induced Ca^{2+} alternans is caused by a feedback loop in which elevated diastolic cytosolic Ca^{2+} leads to increased Ca^{2+}-CaM dependent inactivation of RyR2, reduced SR Ca^{2+} release, SR Ca^{2+} release-uptake imbalance, and decreased diastolic cytosolic Ca^{2+} (Fig. 8). This diastolic cytosolic Ca^{2+} alternation then drives diastolic RyR2 inactivation alternation and Ca^{2+} alternans.

Although cytosolic Ca^{2+} has been suggested in the induction of Ca^{2+} alternans, the role of cytosolic Ca^{2+} in Ca^{2+} alternans and its underlying mechanism are unclear and controversial. Early modeling studies assumed the presence of cytosolic Ca^{2+} dependent-inactivation of RyR2 in simulating Ca^{2+} alternans [49]. However, this is not universally accepted, because in *in vitro* experiments, cytosolic Ca^{2+} in the physiological range does not provide sufficient inactivation of RyR2. Rather, other mechanisms of RyR2 termination have been proposed, such as SR Ca^{2+} depletion or stochastic attrition [50, 51]. Nevertheless, *in vivo* experiments [52] seem to support the idea of a strong inactivation of RyR2 by cytosolic Ca^{2+}. Following these ideas, RyR2 inactivation has been proposed as a possible mechanism for alternans both in modeling [20, 32, 33] and in experimental studies [16, 23, 27, 29, 30]. These studies shed light on how an incomplete recovery of RyR2 from inactivation (or refractoriness) can lead to alternans at fast pacing rates. However, the mechanism of RyR2 inactivation and its relation to the pacing rate are completely undefined. It is this crucial point that the present study has addressed. We demonstrate that pacing induced cytosolic Ca^{2+} elevation increases the Ca^{2+}-CaM complex that induces RyR2 inactivation that drives Ca^{2+} alternans.

Given its significant role in modulating SR Ca^{2+} release, impaired CaM function is expected to be pathological. Indeed, naturally occurring mutations in CaM cause cardiac arrhythmias and sudden death [53]. Impairing CaM inhibition of RyR2 in mice by mutating the CaM binding site in RyR2 also causes cardiac hypertrophy and early death [54]. Reduced CaM binding to RyR2 has also been implicated in heart failure [35, 55]. Thus, these observations suggest that enhancing CaM-RyR2 interaction may represent an effective therapeutic strategy for treating cardiac arrhythmias and heart failure. In support of this idea, it has recently been shown that the GOF CaM-M37Q mutation and enhancing CaM-RyR2 interaction are able to suppress spontaneous SR Ca^{2+} release and catecholaminergic polymorphic ventricular tachycardia (CPVT) [44]. However, as shown in the present study, enhancing CaM function (as in CaM-M37Q mutation) markedly promotes Ca^{2+} alternans that can lead to ventricular fibrillation and sudden death. Given that both enhancing and suppressing CaM function could lead to cardiac arrhythmias, normalizing the activity of CaM would be the key in protecting against CaM-mediated cardiac arrhythmias.

The impact of CaM and CaM mutations on Ca^{2+} dynamics/fluxes in isolated cardiomyocytes has been extensively investigated[38, 44, 56-60]. Surprisingly, little is known about the impact of CaM and CaM

mutations on Ca^{2+} alternans. This is due, in part, to the technical difficulties of studying the effects of altered CaM function on Ca^{2+} alternans in isolated cardiomyocytes or in intact hearts. It is generally difficult to induce stable Ca^{2+} alternans in isolated cultured cardiomyocytes overexpressing CaM or CaM mutants at physiologically relevant pacing frequencies. It is also difficult to study the impact of altered CaM function globally in the intact heart without detrimental effects, given its critical roles in many cellular processes. To circumvent the problems associated with isolated cultured cardiomyocytes and global adverse effects on the heart, we employed a local *in vivo* gene delivery approach by directly injecting adenoviruses expressing CaM or CaM mutants into the anterior wall of the left ventricle. This local expression allows us to assess, for the first time, the impact of altered CaM function on Ca^{2+} alternans and Ca^{2+} transient recovery in cardiomyocytes in the setting of intact hearts. Furthermore, there is evidence suggesting that the induction and mechanism of fast-pacing induced Ca^{2+} alternans in single isolated cardiomyocytes may be different from those in intact hearts. For instance, enhanced RyR2 function has been shown to promote Ca^{2+} alternans in isolated cardiomyocytes where spontaneous Ca^{2+} release events are present [61-63]. In contrast, we showed that enhanced RyR2 function suppresses Ca^{2+} alternans in intact working hearts [28]. Although the exact reason for this difference has yet to be determined, one clear difference between isolated cardiomyocytes and intact hearts is the lack of spontaneous Ca^{2+} release events in intact hearts during fast-pacing that induces Ca^{2+} alternans [28]. Moreover, the stimulation frequency required to trigger Ca^{2+} alternans in intact hearts is much higher than that in isolated cardiomyocytes. These observations suggest that the mechanism that contributes to fast-pacing induced Ca^{2+} alternans in intact hearts may be different from that in isolated cardiomyocytes. Thus, our local *in vivo* gene delivery technique combined with *in situ* intact heart Ca^{2+} imaging represents a more physiologically relevant approach to investigating the role of CaM in Ca^{2+} alternans as compared to the single-cell approach.

In summary, the present study demonstrates that Ca^{2+}-CaM dependent inactivation of RyR2 plays an important role in pacing induced Ca^{2+} alternans in intact hearts. Based on our new findings, we developed a novel numerical myocyte model of Ca^{2+} alternans. The new model recapitulates the impact of altered RyR2 and CaM function on Ca^{2+} alternans under 9 different experimental conditions. Our simulation analyses reveal that pacing-induced diastolic cytosolic Ca^{2+} elevation drives Ca^{2+}-CaM dependent RyR2 inactivation, and that RyR2 inactivation, when sufficiently high, leads to SR Ca^{2+} release-uptake imbalance. This imbalanced Ca^{2+}uptake and release results in alternations in diastolic cytosolic Ca^{2+}, in RyR2 inactivation, and in SR Ca^{2+} release, and thus perpetuation of Ca^{2+} alternans.

Study limitations

Despite the physiological advantages of *in vivo* CaM manipulation and *in situ* intact heart imaging, our intact heart imaging approach does not isolate the effects of altered CaM function on specific CaM targets. Therefore, although RyR2 is a major target of CaM regulation of Ca^{2+} alternans, it is likely that other CaM targets are importantly involved as well. Further studies will be needed to fully understand the roles of different CaM targets in Ca^{2+} alternans in the setting of intact hearts. Given the close coupling between Ca^{2+} alternans and action potential duration (APD) alternans, the role of CaM in APD alternans has yet to be determined. Furthermore, since a mathematical model cannot be used as a definitive proof of a biological function, the fact that our mathematical model reproduces very well the experimental data and supports the notion that CaM-dependent inactivation of RyR2 is a key determinant of Ca^{2+} alternans does not entirely rule out that a variation of the model might also agree with the experiments and explain Ca^{2+} alternans by a different mechanism. An interesting observation in our simulations is that pacing at 9 Hz led to transient alternans, while pacing at 12 Hz resulted in stable

alternans. However, more studies will be required to fully understand the mechanism underlying transient and stable Ca^{2+} alternans at different stimulation frequencies.

ACKNOWLEDGEMENTS

This work was supported by research grants from the Heart and Stroke Foundation of Canada (G-19-0026444), the Heart and Stroke Foundation Chair in Cardiovascular Research (END611955), the Canadian Institutes of Health Research to SRWC (PJT-155940), the Spanish Ministry of Science Innovation and Universities SAF2017-88019-C3-1R, 2R and 3R (to LHM, RB and BE), Marato-TV3 20152030 (to LHM) and 20151110 (to BE), and Generalitat de Catalunya SGR2017-1769 (to LHM).

CONFLICT OF INTEREST

The authors declare that they have no conflicts of interest with the contents of this article.

AUTHOR CONTRIBUTIONS

JW, JY, DB, WG, XZ, BS, RB, LHM, EAL, BE, and SRWC designed the research; JW, JY, DB, WG, XZ, BS, RW, JPE, AV, EAL, and BE performed the research; JW, JY, DB, WG, XZ, BS, AV, RB, LHM, EAL, BE, and SRWC analyzed data; and JW, JY, DB, LHM, EAL, BE, SRWC wrote the paper.

REFERENCES

1. Kapur S, Wasserstrom JA, Kelly JE, Kadish AH and Aistrup GL. Acidosis and ischemia increase cellular Ca^{2+} transient alternans and repolarization alternans susceptibility in the intact rat heart. *American journal of physiologyHeart and circulatory physiology*. 2009;296:H1491-512.
2. Wilson LD, Jeyaraj D, Wan X, Hoeker GS, Said TH, Gittinger M, Laurita KR and Rosenbaum DS. Heart failure enhances susceptibility to arrhythmogenic cardiac alternans. *Heart rhythm : the official journal of the Heart Rhythm Society*. 2009;6:251-259.
3. Giudici MC and Savage MP. Transient pulsus alternans during acute myocardial ischemia and its resolution following beta-adrenergic blockade. *American Heart Journal*. 1990;119:960-962.
4. Verrier RL and Nearing BD. Electrophysiologic basis for T wave alternans as an index of vulnerability to ventricular fibrillation. *Journal of cardiovascular electrophysiology*. 1994;5:445-461.
5. Rosenbaum DS, Jackson LE, Smith JM, Garan H, Ruskin JN and Cohen RJ. Electrical alternans and vulnerability to ventricular arrhythmias. *The New England journal of medicine*. 1994;330:235-241.
6. Escobar AL and Valdivia HH. Cardiac alternans and ventricular fibrillation: a bad case of ryanodine receptors reneging on their duty. *Circulation research*. 2014;114:1369-1371.
7. Kihara Y and Morgan JP. Abnormal Cai^{2+} handling is the primary cause of mechanical alternans: study in ferret ventricular muscles. *The American Journal of Physiology*. 1991;261:H1746-55.
8. Chudin E, Goldhaber J, Garfinkel A, Weiss J and Kogan B. Intracellular Ca^{2+} dynamics and the stability of ventricular tachycardia. *Biophysical journal*. 1999;77:2930-2941.
9. Diaz ME, O'Neill SC and Eisner DA. Sarcoplasmic Reticulum Calcium Content Fluctuation Is the Key to Cardiac Alternans. *Circ Res*. 2004;94:650-656.

10. Laurita KR and Rosenbaum DS. Cellular mechanisms of arrhythmogenic cardiac alternans. *Progress in biophysics and molecular biology*. 2008;97:332-347.
11. Xie LH, Sato D, Garfinkel A, Qu Z and Weiss JN. Intracellular Ca alternans: coordinated regulation by sarcoplasmic reticulum release, uptake, and leak. *Biophysical journal*. 2008;95:3100-3110.
12. Aistrup GL, Shiferaw Y, Kapur S, Kadish AH and Wasserstrom JA. Mechanisms underlying the formation and dynamics of subcellular calcium alternans in the intact rat heart. *Circ Res*. 2009;104:639-49.
13. Wan X, Laurita KR, Pruvot EJ and Rosenbaum DS. Molecular correlates of repolarization alternans in cardiac myocytes. *Journal of Molecular and Cellular Cardiology*. 2005;39:419-428.
14. Eisner DA, Li Y and O'Neill SC. Alternans of intracellular calcium: mechanism and significance. *Heart rhythm : the official journal of the Heart Rhythm Society*. 2006;3:743-745.
15. Laurita KR and Rosenbaum DS. Mechanisms and potential therapeutic targets for ventricular arrhythmias associated with impaired cardiac calcium cycling. *Journal of Molecular and Cellular Cardiology*. 2008;44:31-43.
16. Wang L, Myles RC, De Jesus NM, Ohlendorf AK, Bers DM and Ripplinger CM. Optical mapping of sarcoplasmic reticulum Ca^{2+} in the intact heart: ryanodine receptor refractoriness during alternans and fibrillation. *Circulation research*. 2014;114:1410-1421.
17. Kanaporis G and Blatter LA. The mechanisms of calcium cycling and action potential dynamics in cardiac alternans. *Circulation research*. 2015;116:846-856.
18. Bers DM. Cardiac excitation-contraction coupling. *Nature*. 2002;415:198-205.
19. Cordeiro JM, Malone JE, Di Diego JM, Scornik FS, Aistrup GL, Antzelevitch C and Wasserstrom JA. Cellular and subcellular alternans in the canine left ventricle. *Am J Physiol Heart Circ Physiol*. 2007;293:H3506-16.
20. Alvarez-Lacalle E, Cantalapiedra IR, Penaranda A, Cinca J, Hove-Madsen L and Echebarria B. Dependency of calcium alternans on ryanodine receptor refractoriness. *PloS one*. 2013;8:e55042.
21. Qu Z, Liu MB and Nivala M. A unified theory of calcium alternans in ventricular myocytes. *Scientific reports*. 2016;6:35625.
22. Huser J, Wang YG, Sheehan KA, Cifuentes F, Lipsius SL and Blatter LA. Functional coupling between glycolysis and excitation-contraction coupling underlies alternans in cat heart cells. *The Journal of physiology*. 2000;524 Pt 3:795-806.
23. Picht E, DeSantiago J, Blatter LA and Bers DM. Cardiac alternans do not rely on diastolic sarcoplasmic reticulum calcium content fluctuations. *Circulation research*. 2006;99:740-748.
24. Llach A, Molina CE, Fernandes J, Padro J, Cinca J and Hove-Madsen L. Sarcoplasmic reticulum and L-type Ca(2)(+) channel activity regulate the beat-to-beat stability of calcium handling in human atrial myocytes. *The Journal of physiology*. 2011;589:3247-3262.
25. Molina CE, Llach A, Herraiz-Martinez A, Tarifa C, Barriga M, Wiegerinck RF, Fernandes J, Cabello N, Vallmitjana A, Benitez R, Montiel J, Cinca J and Hove-Madsen L. Prevention of adenosine A2A receptor activation diminishes beat-to-beat alternation in human atrial myocytes. *Basic research in cardiology*. 2016;111:5-015-0525-2. Epub 2015 Nov 26.
26. Diaz ME, Eisner DA and O'Neill SC. Depressed Ryanodine Receptor Activity Increases Variability and Duration of the Systolic Ca^{2+} Transient in Rat Ventricular Myocytes. *Circ Res*. 2002;91:585-593.
27. Zhong X, Sun B, Vallmitjana A, Mi T, Guo W, Ni M, Wang R, Guo A, Duff HJ, Gillis AM, Song LS, Hove-Madsen L, Benitez R and Chen SR. Suppression of ryanodine receptor

function prolongs Ca^{2+} release refractoriness and promotes cardiac alternans in intact hearts. *Biochem J*. 2016;473:3951-3964.
28. Sun B, Wei J, Zhong X, Guo W, Yao J, Wang R, Vallmitjana A, Benitez R, Hove-Madsen L and Chen SRW. The cardiac ryanodine receptor, but not sarcoplasmic reticulum Ca^{2+}-ATPase, is a major determinant of Ca^{2+} alternans in intact mouse hearts. *J Biol Chem*. 2018.
29. Shkryl VM, Maxwell JT, Domeier TL and Blatter LA. Refractoriness of sarcoplasmic reticulum Ca^{2+} release determines Ca^{2+} alternans in atrial myocytes. *American journal of physiologyHeart and circulatory physiology*. 2012;302:H2310-20.
30. Lugo CA, Cantalapiedra IR, Penaranda A, Hove-Madsen L and Echebarria B. Are SR Ca content fluctuations or SR refractoriness the key to atrial cardiac alternans?: insights from a human atrial model. *American journal of physiologyHeart and circulatory physiology*. 2014;306:H1540-52.
31. Restrepo JG, Weiss JN and Karma A. Calsequestrin-mediated mechanism for cellular calcium transient alternans. *Biophys J*. 2008;95:3767-89.
32. Rovetti R, Cui X, Garfinkel A, Weiss JN and Qu Z. Spark-induced sparks as a mechanism of intracellular calcium alternans in cardiac myocytes. *Circ Res*. 2010;106:1582-91.
33. Cantalapiedra IR, Alvarez-Lacalle E, Penaranda A and Echebarria B. Minimal model for calcium alternans due to SR release refractoriness. *Chaos (Woodbury, NY)*. 2017;27:093928.
34. Yamaguchi N, Xu L, Pasek DA, Evans KE and Meissner G. Molecular basis of calmodulin binding to cardiac muscle Ca^{2+} release channel (ryanodine receptor). *The Journal of biological chemistry*. 2003;278:23480-23486.
35. Yang Y, Guo T, Oda T, Chakraborty A, Chen L, Uchinoumi H, Knowlton AA, Fruen BR, Cornea RL, Meissner G and Bers DM. Cardiac myocyte Z-line calmodulin is mainly RyR2-bound, and reduction is arrhythmogenic and occurs in heart failure. *Circ Res*. 2014;114:295-306.
36. Gong D, Chi X, Wei J, Zhou G, Huang G, Zhang L, Wang R, Lei J, Chen SRW and Yan N. Modulation of cardiac ryanodine receptor 2 by calmodulin. *Nature*. 2019;572:347-351.
37. Tian X, Tang Y, Liu Y, Wang R and Chen SR. Calmodulin modulates the termination threshold for cardiac ryanodine receptor-mediated Ca^{2+} release. *The Biochemical journal*. 2013;455:367-375.
38. Kryshtal DO, Gryshchenko O, Gomez-Hurtado N and Knollmann BC. Impaired calcium-calmodulin-dependent inactivation of Cav1.2 contributes to loss of sarcoplasmic reticulum calcium release refractoriness in mice lacking calsequestrin 2. *J Mol Cell Cardiol*. 2015;82:75-83.
39. Belke DD, Gloss B, Hollander JM, Swanson EA, Duplain H and Dillmann WH. In vivo gene delivery of HSP70i by adenovirus and adeno-associated virus preserves contractile function in mouse heart following ischemia-reperfusion. *Am J Physiol Heart Circ Physiol*. 2006;291:H2905-10.
40. Chen B, Guo A, Gao Z, Wei S, Xie YP, Chen SR, Anderson ME and Song LS. In situ confocal imaging in intact heart reveals stress-induced Ca^{2+} release variability in a murine catecholaminergic polymorphic ventricular tachycardia model of type 2 ryanodine receptor(R4496C+/-) mutation. *CirculationArrhythmia and electrophysiology*. 2012;5:841-849.
41. Bai Y, Jones PP, Guo J, Zhong X, Clark RB, Zhou Q, Wang R, Vallmitjana A, Benitez R, Hove-Madsen L, Semeniuk L, Guo A, Song LS, Duff HJ and Chen SR. Phospholamban knockout breaks arrhythmogenic Ca^{2+} waves and suppresses catecholaminergic polymorphic ventricular tachycardia in mice. *Circulation research*. 2013;113:517-526.
42. Zhang PC, Llach A, Sheng XY, Hove-Madsen L and Tibbits GF. Calcium handling in zebrafish ventricular myocytes. *Am J Physiol Regul Integr Comp Physiol*. 2011;300:R56-66.

43. Bondarenko VE, Szigeti GP, Bett GC, Kim SJ and Rasmusson RL. Computer model of action potential of mouse ventricular myocytes. *Am J Physiol Heart Circ Physiol*. 2004;287:H1378-403.
44. Liu B, Walton SD, Ho HT, Belevych AE, Tikunova SB, Bonilla I, Shettigar V, Knollmann BC, Priori SG, Volpe P, Radwanski PB, Davis JP and Gyorke S. Gene Transfer of Engineered Calmodulin Alleviates Ventricular Arrhythmias in a Calsequestrin-Associated Mouse Model of Catecholaminergic Polymorphic Ventricular Tachycardia. *Journal of the American Heart Association*. 2018;7.
45. Gomez-Hurtado N, Boczek NJ, Kryshtal DO, Johnson CN, Sun J, Nitu FR, Cornea RL, Chazin WJ, Calvert ML, Tester DJ, Ackerman MJ and Knollmann BC. Novel CPVT-Associated Calmodulin Mutation in CALM3 (CALM3-A103V) Activates Arrhythmogenic Ca Waves and Sparks. *Circulation Arrhythmia and electrophysiology*. 2016;9.
46. Peterson BZ, DeMaria CD, Adelman JP and Yue DT. Calmodulin is the Ca^{2+} sensor for Ca^{2+} -dependent inactivation of L- type calcium channels [published erratum appears in Neuron 1999 Apr;22(4):following 893]. *Neuron*. 1999;22:549-558.
47. Chen W, Wang R, Chen B, Zhong X, Kong H, Bai Y, Zhou Q, Xie C, Zhang J, Guo A, Tian X, Jones PP, O'Mara ML, Liu Y, Mi T, Zhang L, Bolstad J, Semeniuk L, Cheng H, Zhang J, Chen J, Tieleman DP, Gillis AM, Duff HJ, Fill M, Song LS and Chen SR. The ryanodine receptor store-sensing gate controls Ca^{2+} waves and Ca^{2+}-triggered arrhythmias. *Nature medicine*. 2014;20:184-192.
48. Jiang D, Xiao B, Yang D, Wang R, Choi P, Zhang L, Cheng H and Chen SRW. RyR2 mutations linked to ventricular tachycardia and sudden death reduce the threshold for store-overload-induced Ca^{2+} release (SOICR). *ProcNatlAcadSciUSA*. 2004;101:13062-13067.
49. Stern MD, Song LS, Cheng H, Sham JS, Yang HT, Boheler KR and Rios E. Local control models of cardiac excitation-contraction coupling. A possible role for allosteric interactions between ryanodine receptors. *J Gen Physiol*. 1999;113:469-489.
50. Lukyanenko V, Wiesner TF and Gyorke S. Termination of Ca^{2+} release during Ca^{2+} sparks in rat ventricular myocytes. *The Journal of physiology*. 1998;507 (Pt 3):667-677.
51. Stern MD and Cheng H. Putting out the fire: what terminates calcium-induced calcium release in cardiac muscle? *Cell calcium*. 2004;35:591-601.
52. Sham JS, Song LS, Chen Y, Deng LH, Stern MD, Lakatta EG and Cheng H. Termination of Ca^{2+} release by a local inactivation of ryanodine receptors in cardiac myocytes. *Proc Natl Acad Sci U S A*. 1998;95:15096-15101.
53. Nyegaard M, Overgaard MT, Sondergaard MT, Vranas M, Behr ER, Hildebrandt LL, Lund J, Hedley PL, Camm AJ, Wettrell G, Fosdal I, Christiansen M and Borglum AD. Mutations in calmodulin cause ventricular tachycardia and sudden cardiac death. *American Journal of Human Genetics*. 2012;91:703-712.
54. Yamaguchi N, Takahashi N, Xu L, Smithies O and Meissner G. Early cardiac hypertrophy in mice with impaired calmodulin regulation of cardiac muscle Ca release channel. *The Journal of clinical investigation*. 2007;117:1344-1353.
55. Ono M, Yano M, Hino A, Suetomi T, Xu X, Susa T, Uchinoumi H, Tateishi H, Oda T, Okuda S, Doi M, Kobayashi S, Yamamoto T, Koseki N, Kyushiki H, Ikemoto N and Matsuzaki M. Dissociation of calmodulin from cardiac ryanodine receptor causes aberrant Ca^{2+} release in heart failure. *Cardiovasc Res*. 2010;87:609-17.
56. Zuhlke RD, Pitt GS, Deisseroth K, Tsien RW and Reuter H. Calmodulin supports both inactivation and facilitation of L-type calcium channels [see comments]. *Nature*. 1999;399:159-162.

57. Alseikhan BA, DeMaria CD, Colecraft HM and Yue DT. Engineered calmodulins reveal the unexpected eminence of Ca^{2+} channel inactivation in controlling heart excitation. *Proceedings of the National Academy of Sciences of the United States of America*. 2002;99:17185-17190.
58. Yang D, Song LS, Zhu WZ, Chakir K, Wang W, Wu C, Wang Y, Xiao RP, Chen SRW and Cheng H. Calmodulin Regulation of Excitation-Contraction Coupling in Cardiac Myocytes. *Circ Res*. 2003;92:659-667.
59. Boczek NJ, Gomez-Hurtado N, Ye D, Calvert ML, Tester DJ, Kryshtal D, Hwang HS, Johnson CN, Chazin WJ, Loporcaro CG, Shah M, Papez AL, Lau YR, Kanter R, Knollmann BC and Ackerman MJ. Spectrum and Prevalence of CALM1-, CALM2-, and CALM3-Encoded Calmodulin Variants in Long QT Syndrome and Functional Characterization of a Novel Long QT Syndrome-Associated Calmodulin Missense Variant, E141G. *Circ Cardiovasc Genet*. 2016;9:136-146.
60. Limpitikul WB, Dick IE, Tester DJ, Boczek NJ, Limphong P, Yang W, Choi MH, Babich J, DiSilvestre D, Kanter RJ, Tomaselli GF, Ackerman MJ and Yue DT. A Precision Medicine Approach to the Rescue of Function on Malignant Calmodulinopathic Long-QT Syndrome. *Circulation research*. 2017;120:39-48.
61. Belevych AE, Terentyev D, Viatchenko-Karpinski S, Terentyeva R, Sridhar A, Nishijima Y, Wilson LD, Cardounel AJ, Laurita KR, Carnes CA, Billman GE and Gyorke S. Redox modification of ryanodine receptors underlies calcium alternans in a canine model of sudden cardiac death. *Cardiovasc Res*. 2009;84:387-95.
62. Xie W, Santulli G, Guo X, Gao M, Chen BX and Marks AR. Imaging atrial arrhythmic intracellular calcium in intact heart. *J Mol Cell Cardiol*. 2013;64:120-3.
63. Kang G, Giovannone SF, Liu N, Liu FY, Zhang J, Priori SG and Fishman GI. Purkinje cells from RyR2 mutant mice are highly arrhythmogenic but responsive to targeted therapy. *Circulation research*. 2010;107:512-519.
64. Sikkel MB, Francis DP, Howard J, Gordon F, Rowlands C, Peters NS, Lyon AR, Harding SE and MacLeod KT. Hierarchical statistical techniques are necessary to draw reliable conclusions from analysis of isolated cardiomyocyte studies. *Cardiovasc Res*. 2017;113:1743-1752.
65. Zhou Q, Xiao J, Jiang D, Wang R, Vembaiyan K, Wang A, Smith CD, Xie C, Chen W, Zhang J, Tian X, Jones PP, Zhong X, Guo A, Chen H, Zhang L, Zhu W, Yang D, Li X, Chen J, Gillis AM, Duff HJ, Cheng H, Feldman AM, Song LS, Fill M, Back TG and Chen SR. Carvedilol and its new analogs suppress arrhythmogenic store overload-induced Ca^{2+} release. *Nature medicine*. 2011;17:1003-1009.
66. Jiang D, Xiao B, Zhang L and Chen SR. Enhanced basal activity of a cardiac Ca^{2+} release channel (ryanodine receptor) mutant associated with ventricular tachycardia and sudden death. *Circ Res*. 2002;91:218-25.
67. Keizer J and Levine L. Ryanodine receptor adaptation and Ca^{2+}-induced Ca^{2+} release-dependent Ca^{2+} oscillations. *Biophys J*. 1996;71:3477-3487.
68. Jafri MS, Rice JJ and Winslow RL. Cardiac Ca^{2+} dynamics: the roles of ryanodine receptor adaptation and sarcoplasmic reticulum load [published erratum appears in iophys 1998 Jun;74(6):3313]. *Biophys J*. 1998;74:1149-1168.
69. Jones PP, Guo W and Chen SRW. Control of cardiac ryanodine receptor by sarcoplasmic reticulum luminal Ca(2). *J Gen Physiol*. 2017;149:867-875.
70. Shannon TR, Ginsburg KS and Bers DM. Potentiation of fractional sarcoplasmic reticulum calcium release by total and free intra-sarcoplasmic reticulum calcium concentration. *Biophys J*. 2000;78:334-43.

71. Cortassa S, Aon MA, O'Rourke B, Jacques R, Tseng HJ, Marban E and Winslow RL. A computational model integrating electrophysiology, contraction, and mitochondrial bioenergetics in the ventricular myocyte. *Biophys J*. 2006;91:1564-89.

FIGURES AND FIGURE LEGENDS

Fig. 1

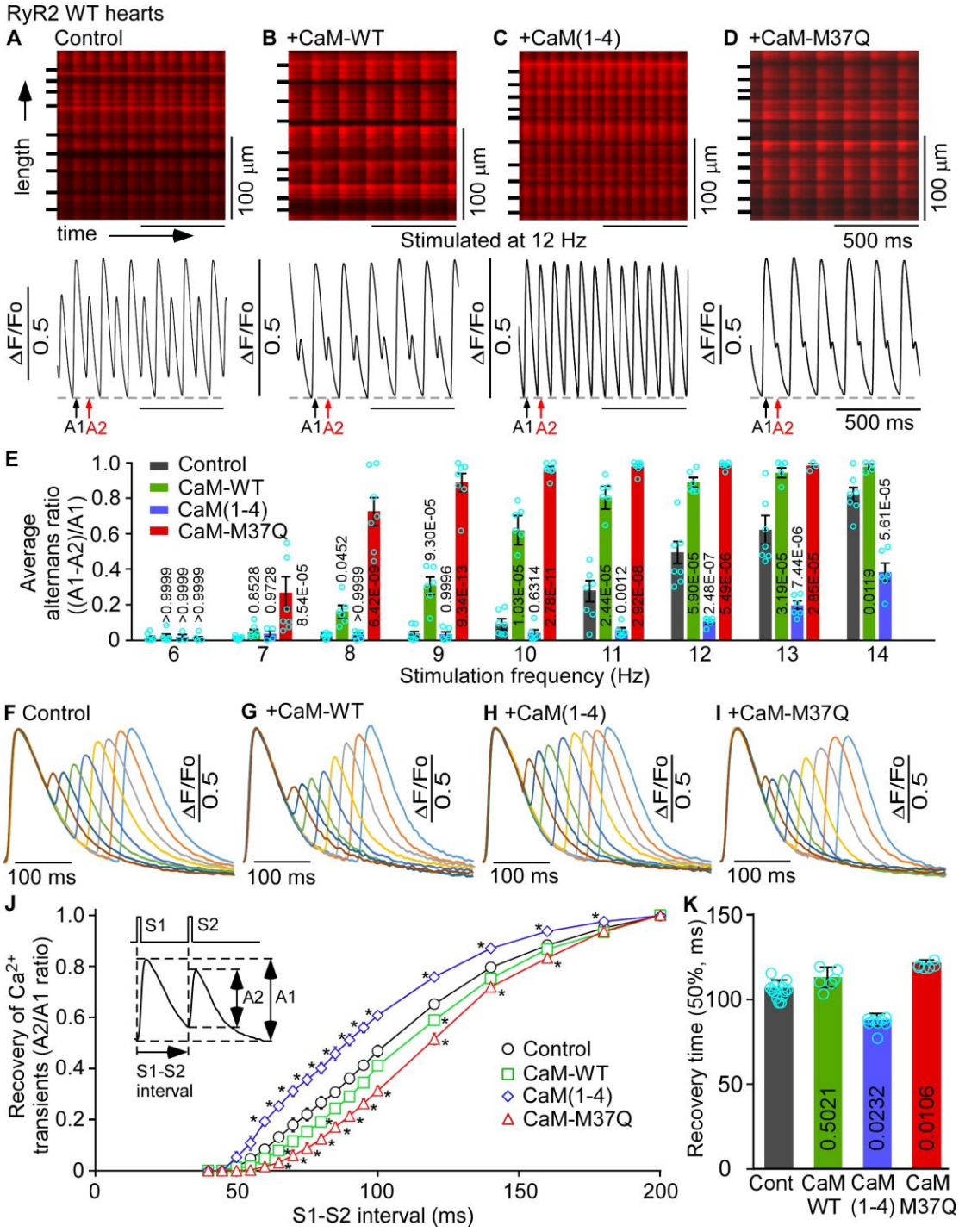

Figure 1. Effects of altered CaM function on Ca^{2+} alternans and Ca^{2+} transient recovery in intact RyR2 WT hearts.

RyR2 WT hearts without injection (**A**, control) or locally injected with adenoviruses expressing CaM-WT (**B**), CaM (1-4) (**C**) or CaM-M37Q (**D**) were loaded with Rhod-2 AM. Ca^{2+} transients in intact

Rhod-2 AM loaded hearts were elicited by pacing at different frequencies (6 to 14 Hz), and recorded using line-scanning confocal imaging. Cell boundaries were indicated by short bars to the left. The ΔF/Fo traces depict the average fluorescence signal of the scan area. (**E**) Alternans ratios for each cell that displayed alternans in the scan area were determined and averaged per cell to yield the average alternans ratio. Alternans ratio is defined as the ratio of the difference in amplitude between the large and small Ca^{2+} transients over the amplitude of the large Ca^{2+} transient. Data are mean ± s.e.m. (n = 7 hearts for Control, 6 hearts for CaM-WT, 6 hearts for CaM (1-4), and 7 hearts for CaM-M37Q with their P values indicated for each condition vs control). To determine the recovery of Ca^{2+} transients, control (**F**), CaM-WT (**G**), CaM (1-4) (**H**) or CaM-M37Q (**I**) adenovirus injected hearts were first stimulated at 5 Hz for 30 beats (S1), followed by a single S2 stimulation. A series of S1S2 stimulations were repeatedly applied with progressively reduced S1S2 intervals from 200 to 40 ms. Ca^{2+} transients were recorded using line-scanning confocal imaging. (**J**) The relationship between A2/A1 ratio of the Ca^{2+} transient amplitude and the S1S2 interval (*$p<0.05$ vs control). (**K**) The 50% recovery time of the Ca^{2+} transient amplitude after pacing with the S1S2 protocol. Data are mean ± s.e.m. (n = 13 hearts for Control, 6 hearts for CaM-WT, 8 hearts for CaM (1-4), and 6 hearts for CaM-M37Q with their P values indicated for each condition vs control) (Two-way ANOVA with Dunnett's post-hoc test for obtaining the adjusted p-values shown in (**E**, **J**), and Kruskal-Wallis test with Dunn's post-hoc test for obtaining the adjusted p-values shown in (**K**), all conditions vs control).

Fig. 2

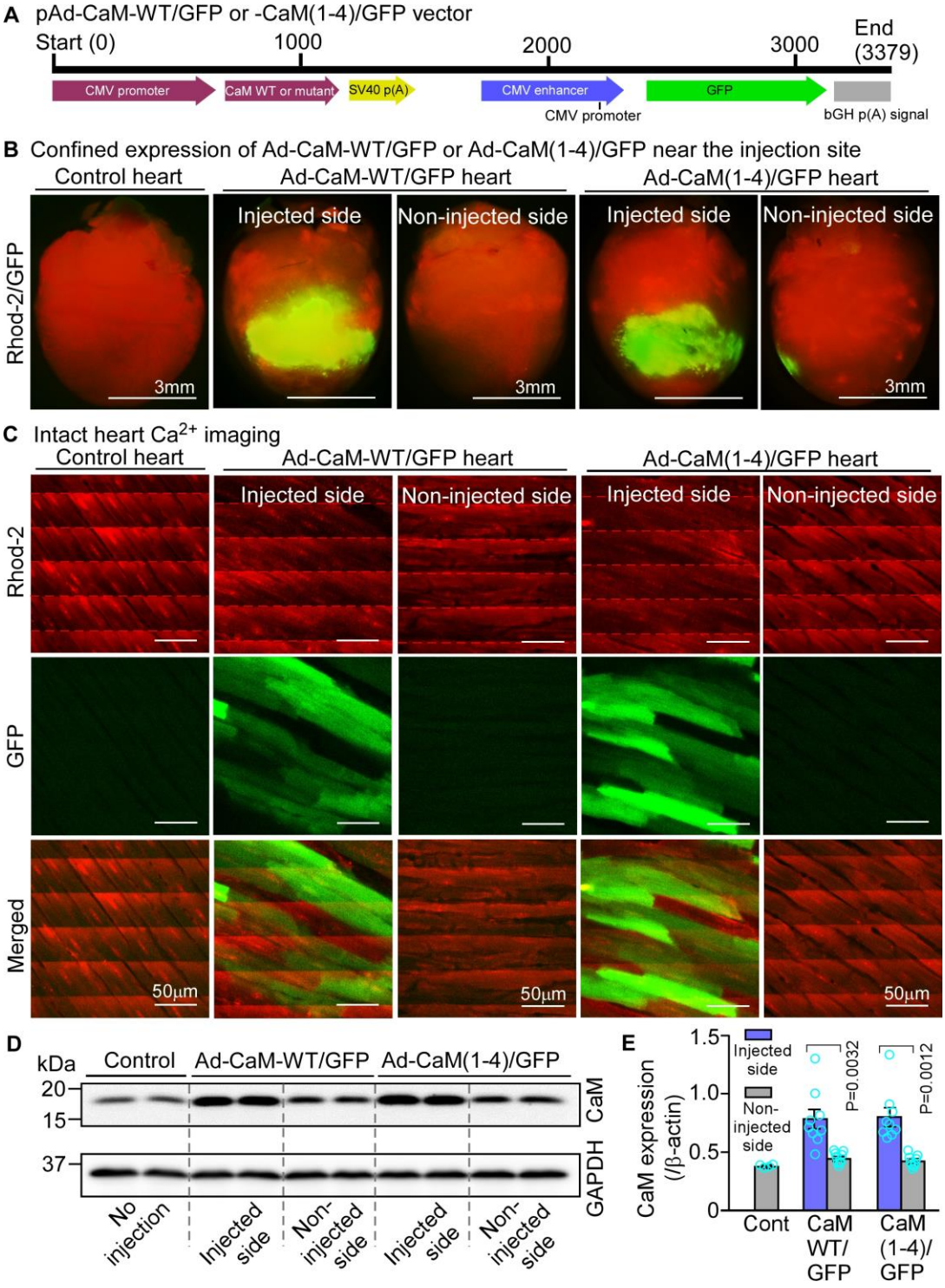

Figure 2. Local expression of CaM-WT/GFP and CaM (1-4)/GFP in intact hearts after in vivo adenovirus-mediated gene delivery.

(**A**) A schematic diagram of plasmids used to produce the adeno-associated viruses (AAV) co-expressing CaM-WT/GFP or CaM(1-4)/GFP. (**B**) Merged Rhod-2 (red) and GFP (green) fluorescent

images of control hearts, hearts injected with Ad-CaM-WT/GFP (injected side vs non-injected side), and hearts injected with Ad-CaM(1-4)/GFP (injected side vs non-injected side), showing locally confined expression of Ad-CaM-WT/GFP or Ad-CaM(1-4)/GFP near the injection site. Scale bars, 3 mm. (**C**) Confocal line-scan x-y Rhod-2, GFP, or merged images of control hearts or hearts injected with Ad-CaM-WT/GFP or Ad-CaM(1-4)/GFP (injected side vs non-injected side) paced at 5 Hz. Red dash-lines indicate Ca^{2+} transients. Scale bars, 50 μm. (**D**) Immunoblotting of tissues isolated from the anterior wall of the left ventricle of control hearts (no injection) or from the left ventricular anterior wall around the sites of injection (injected sites) of CaM-WT/GFP or CaM (1-4)/GFP adenoviruses or from the posterior wall (away from the injection sites, non-injected sites) of the left ventricle. (**E**) Quantification of CaM expression 5 days post adenoviral injection. Data are mean ± s.e.m. (n = 4 hearts for control, 9 hearts for CaM-WT/GFP, and 8 hearts for CaM(1-4)/GFP) (paired Student's *t*-test, injected side vs non-injected site).

Fig. 3

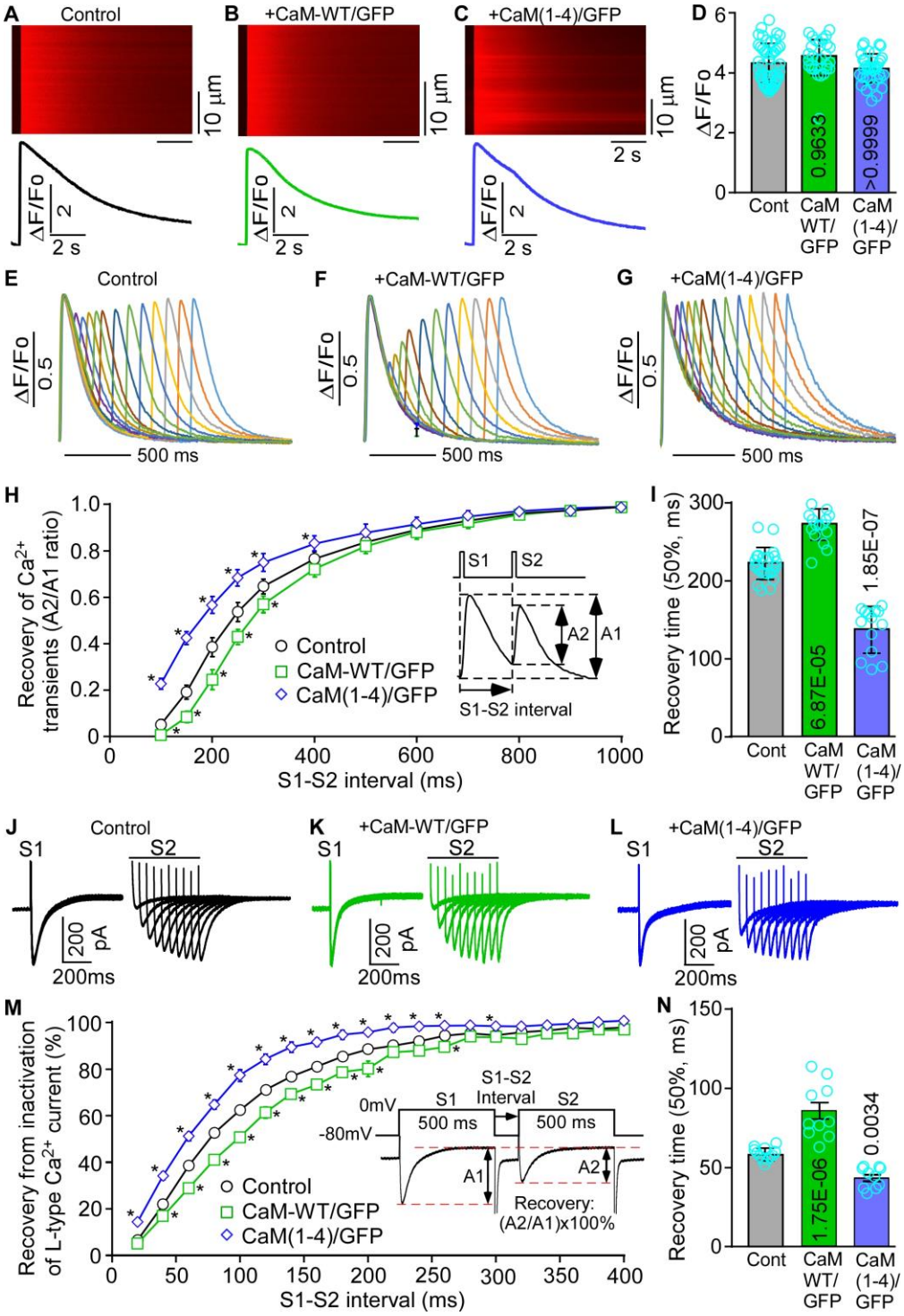

Figure 3. Effects of altered CaM function on SR Ca^{2+} content, recovery of Ca^{2+} transients, and recovery from inactivation of L-type Ca^{2+} current

Sarcoplasmic reticulum (SR) Ca^{2+} contents in Rhod-2 AM loaded mouse ventricular myocytes isolated from RyR2 WT hearts without injection (control) (**A**), or from WT hearts locally injected with Ad-CaM-

WT/GFP (**B**) or Ad-CaM(1-4)/GFP (**C**) were determined by measuring the amplitude of caffeine (20 mM)-induced Ca^{2+} release (**D**). Data are mean ± s.e.m. (n = 47 cells from 10 hearts for control, 28 cells, 5 hearts for CaM-WT/GFP, and 34 cells, 6 hearts for CaM(1-4)/GFP with their P values indicated for each condition vs control). To determine the recovery of Ca^{2+} transients, control (**E**), CaM-WT/GFP (**F**) or CaM (1-4)/GFP (**G**) expressing ventricular myocytes were first stimulated at 1 Hz for 10 beats (S1), followed by a single S2 stimulation. A series of S1S2 stimulations were repeatedly applied with progressively reduced S1S2 intervals from 1000 to 100 ms. Ca^{2+} transients were recorded using line-scanning confocal imaging. (**H**) The relationship between A2/A1 ratio of the Ca^{2+} transient amplitude and S1S2 interval. (**I**) The 50% recovery time of the Ca^{2+} transient amplitude after pacing with the S1S2 protocol. Data are mean ± s.e.m. (n = 24 cells from 8 hearts for control, 15 cells, 6 hearts for CaM-WT/GFP, and 14 cells, 5 hearts for CaM(1-4)/GFP with their P values indicated for each condition vs control). To assess the recovery from inactivation of the L-type Ca^{2+} current, ventricular myocytes isolated from control hearts (**J**), CaM-WT/GFP (**K**) or CaM (1-4)/GFP (**L**) adenovirus injected hearts were first stimulated at 1 Hz for 5 beats (S1), followed by a single S2 stimulation. A series of S1S2 stimulations were repeatedly applied with progressively increased S1S2 intervals from 20 to 400 ms. L-type Ca^{2+} currents were recorded using whole cell patch-clamp recording. (**M**) The relationship between A2/A1 ratio of the L-type Ca^{2+} current amplitude and the S1S2 interval (*$p<0.05$ vs control). (**N**) The 50% recovery time of L-type Ca^{2+} current for control, CaM-WT/GFP or CaM (1-4)/GFP expressing cells. Data are mean ± s.e.m. (n = 12 cells from 5 hearts for Control, 10 cells from 5 hearts for CaM-WT/GFP, 10 cells from 5 hearts for CaM(1-4)/GFP with their P values indicated for each condition vs control) (Values of s.e.m. were adjusted with the hierarchical statistical method [64], One-way ANOVA with Bonferroni's post-hoc test for obtaining the adjusted p-values shown in (**D, H**, **I**, M, **N**), all conditions vs control).

Fig. 4

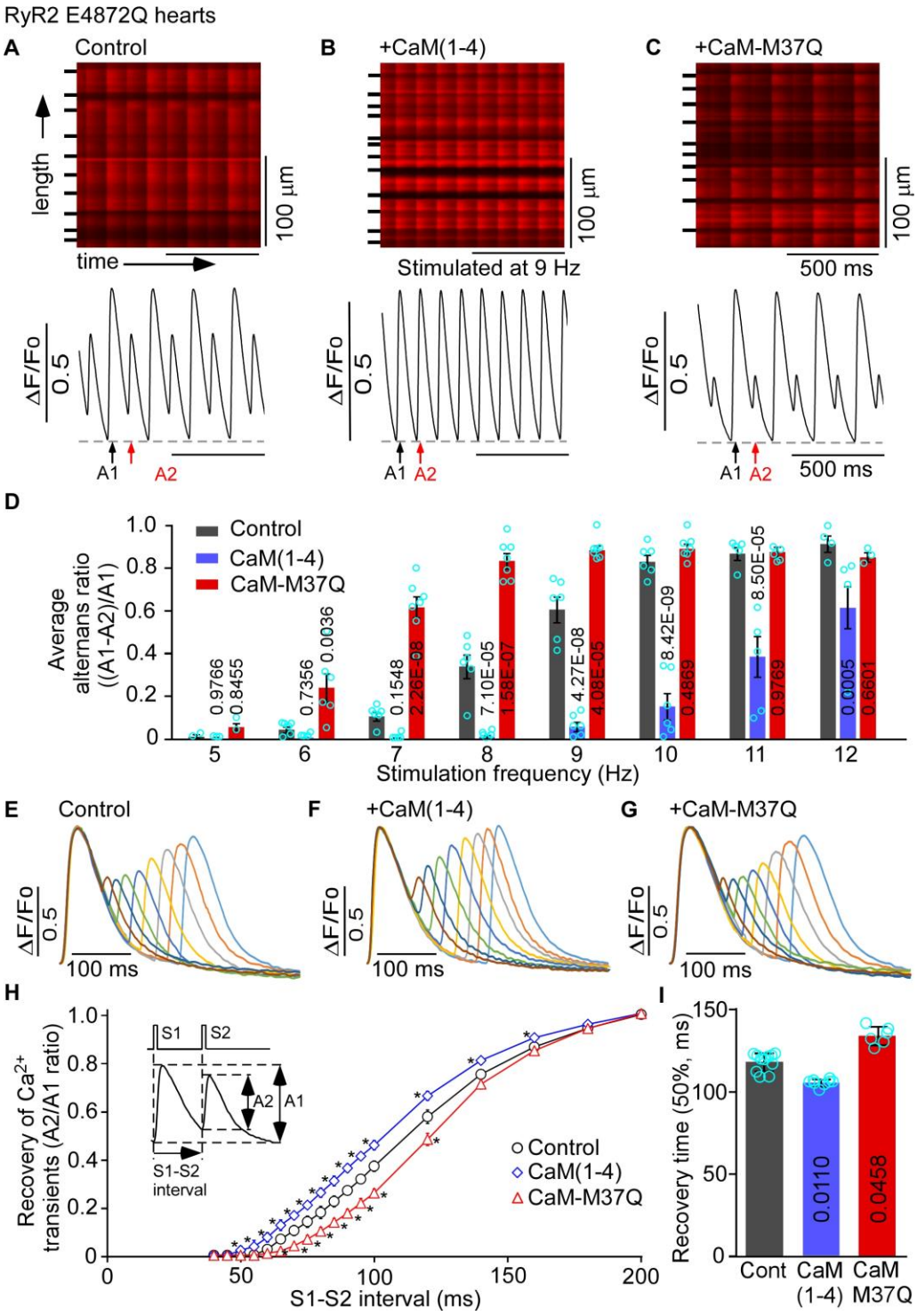

Figure 4. Effects of CaM mutations on Ca^{2+} alternans and Ca^{2+} transient recovery in intact RyR2-E4872Q mutant hearts.

RyR2-E4872Q mutant hearts without injection (**A**, Control) and with local injection of CaM (1-4) (**B**) or CaM-M37Q (**C**) adenoviruses were stimulated at increasing frequencies (5-12 Hz). (**D**) Alternans ratios.

Data are mean ± s.e.m. (n = 6 hearts for Control, 6 hearts for CaM (1-4), and 7 hearts for CaM-M37Q with their P values indicated for each condition vs control). Recovery of Ca^{2+} transients in control (**E**), CaM(1-4) (**F**) or CaM-M37Q (**G**) hearts. (**H**) The relationship between A2/A1 ratio of the Ca^{2+} transient amplitude and the S1S2 interval (*p<0.05 vs control). (**I**) The 50% recovery time of the Ca^{2+} transient amplitude after pacing with the S1S2 protocol. Data are mean ± s.e.m. (n = 11 hearts for Control, 8 hearts for CaM (1-4), and 6 hearts for CaM-M37Q with their P values indicated for each condition vs control) (Two-way ANOVA with Dunnett's post-hoc test for obtaining the adjusted p-values shown in (**D**, **H**), Kruskal-Wallis test with Dunn's post-hoc test for obtaining the adjusted p-values shown in (**I**), all conditions vs control).

Fig. 5

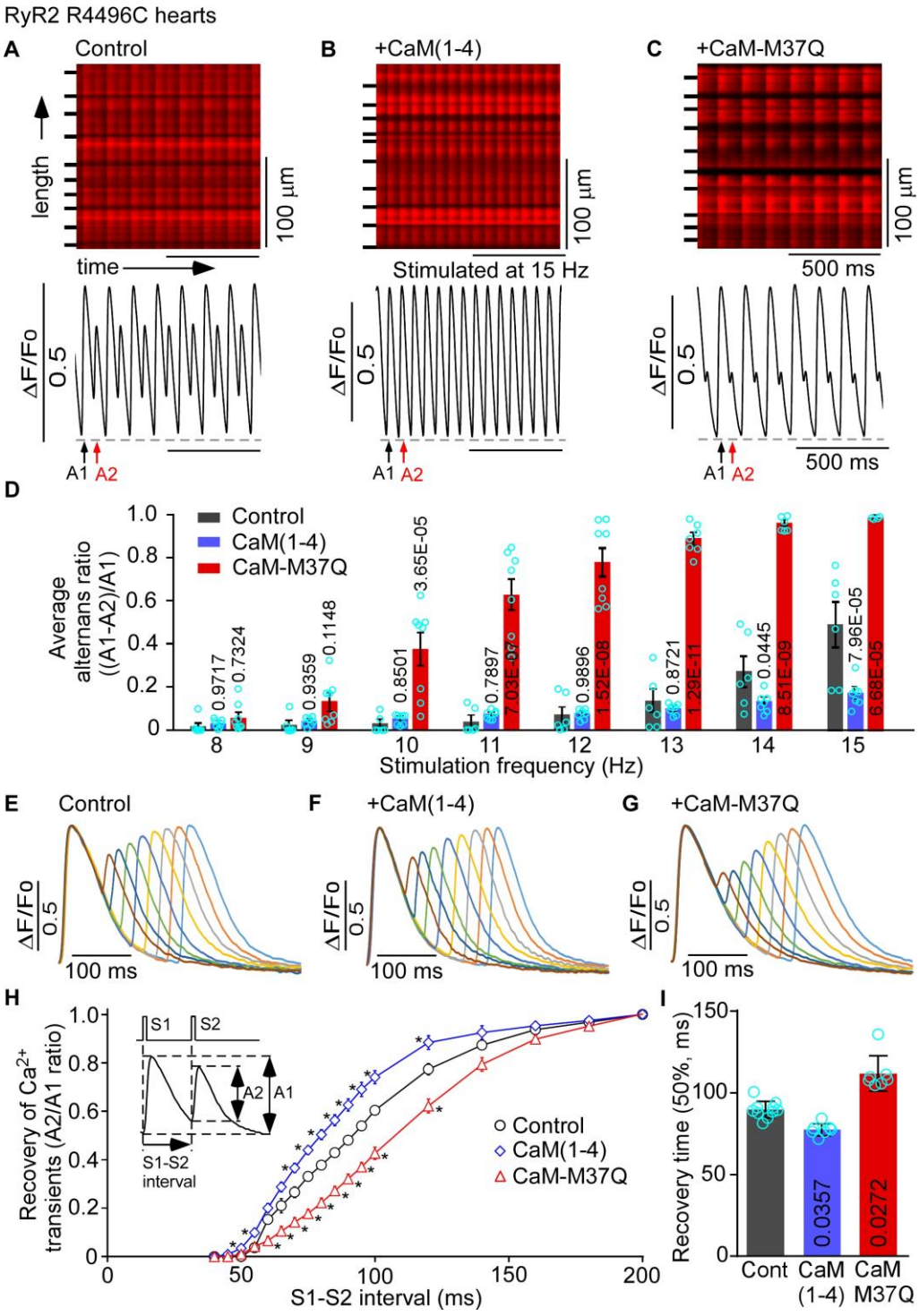

Figure 5. Effects of CaM mutations on Ca^{2+} alternans and Ca^{2+} transient recovery in intact RyR2-R4496C mutant hearts.

RyR2-R4496C mutant hearts without injection (**A**, Control) and with local injection of CaM (1-4) (**B**) or CaM-M37Q (**C**) adenoviruses were stimulated at increasing frequencies (8-15 Hz). (**D**) Alternans ratios.

Data are mean ± s.e.m. (n = 6 hearts for Control, 7 hearts for CaM (1-4), and 8 hearts for CaM-M37Q with their P values indicated for each condition vs control). Recovery of Ca^{2+} transients in control (**E**), CaM (1-4) (**F**) or CaM-M37Q (**G**) hearts. (**H**) The relationship between A2/A1 ratio of the Ca^{2+} transient amplitude and the S1S2 interval (*p<0.05 vs control). (**I**) The 50% recovery time of the Ca^{2+} transient amplitude after pacing with the S1S2 protocol. Data are mean ± s.e.m. (n = 10 hearts for Control, 7 hearts for CaM (1-4), and 7 hearts for CaM-M37Q with their P values indicated for each condition vs control) (Two-way ANOVA with Dunnett's post-hoc test for obtaining the adjusted p-values shown in (**D**, **H**), Kruskal-Wallis test with Dunn's post-hoc test for obtaining the adjusted p-values shown in (**I**), all conditions vs control).

Fig. 6

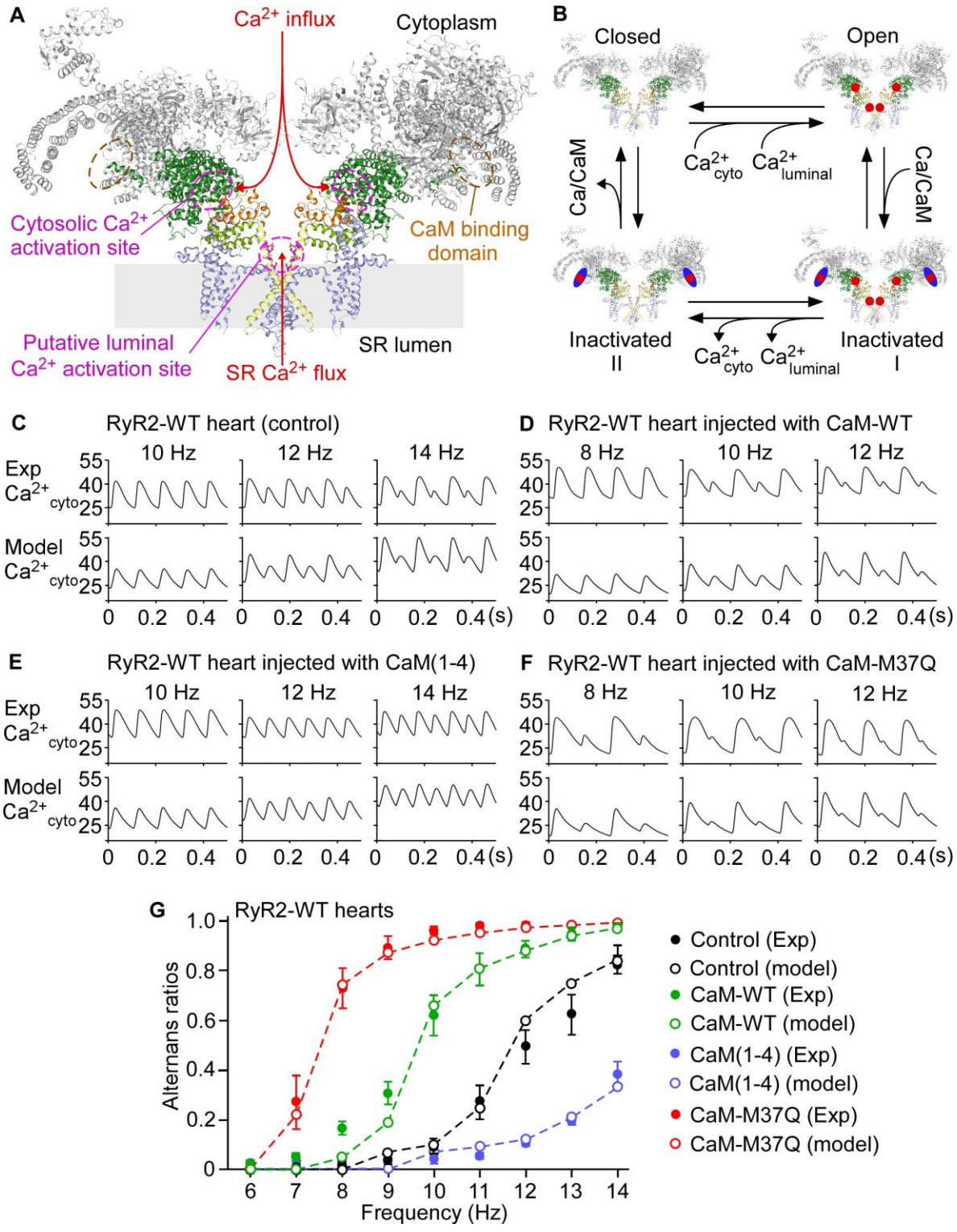

Figure 6. Numerical simulation of altered CaM function on Ca^{2+} alternans in RyR2 WT hearts

(**A**) The three-dimensional structure of RyR2 [36] showing the locations of the cytosolic Ca^{2+} activation sites, the CaM binding site, and the putative luminal Ca^{2+} activation sites. For clarity, only two RyR2

subunits are shown. (**B**) The four-state model of RyR2. The RyR2 presents Ca^{2+} binding domains to both cytosolic and luminal Ca^{2+}, that activate the channel, and to CaM, that inactivates it. Inactivation of the RyR2 occurs as Ca^{2+} binds to CaM at the CaM binding site of the RyR2. There is a second inactivated state that corresponds to a RyR2 with Ca^{2+} bound to the CaM binding site, but not to the cytosolic and luminal activation sites (Supplementary Materials). The model was paced at several stimulation frequencies, obtaining a very good agreement with the experimental traces (**C**). The same procedure was followed for cells injected with CaM-WT (**D**), LOF CaM mutation CaM (1-4) (**E**), and GOF CaM mutant (M37Q) (**F**). (**G**) Comparison of the numerically obtained amplitude of alternans in the four cases with the experimental results, showing a very good agreement.

Fig. 7

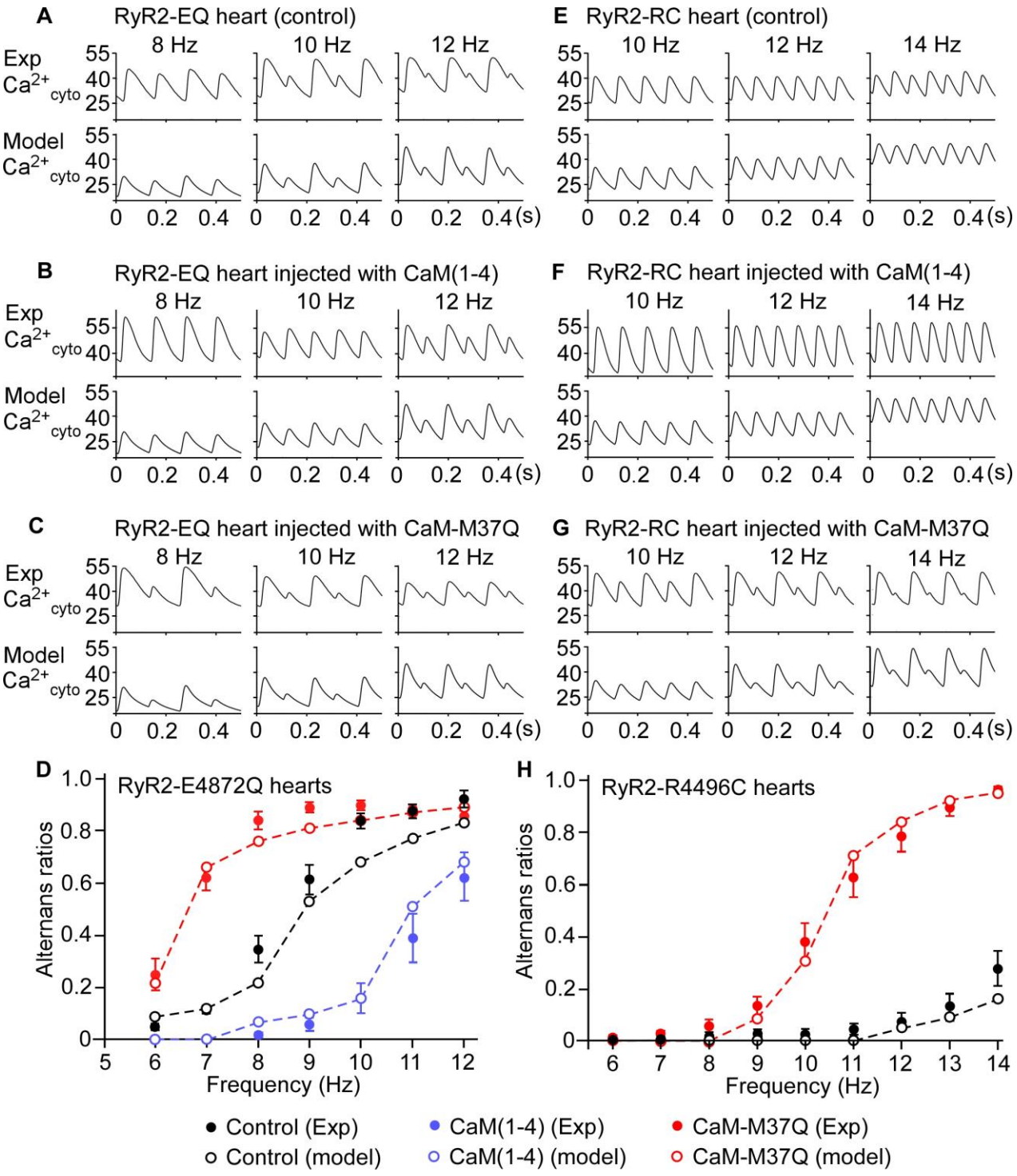

Figure 7. Numerical simulation of altered CaM function on Ca^{2+} alternans in RyR2-E4872Q and RyR2-R4496C mutant hearts

Comparison of numerical and experimental Ca^{2+} traces (concentration of Ca^{2+} bound to Rhod-2) for RyR2-E4872Q (**A**) and RyR2-R4496C (**E**) mutant hearts. The model reproduces very well the

dynamics, both in the control case and with injected LOF CaM (1-4) (**B**, **F**), and GOF CaM-M37Q (**C**, **G**) mutants. The measured amplitudes agree very well in all cases for the RyR2-E4872Q (**D**) and RyR2-R4496C (**H**) mutant hearts.

Fig. 8

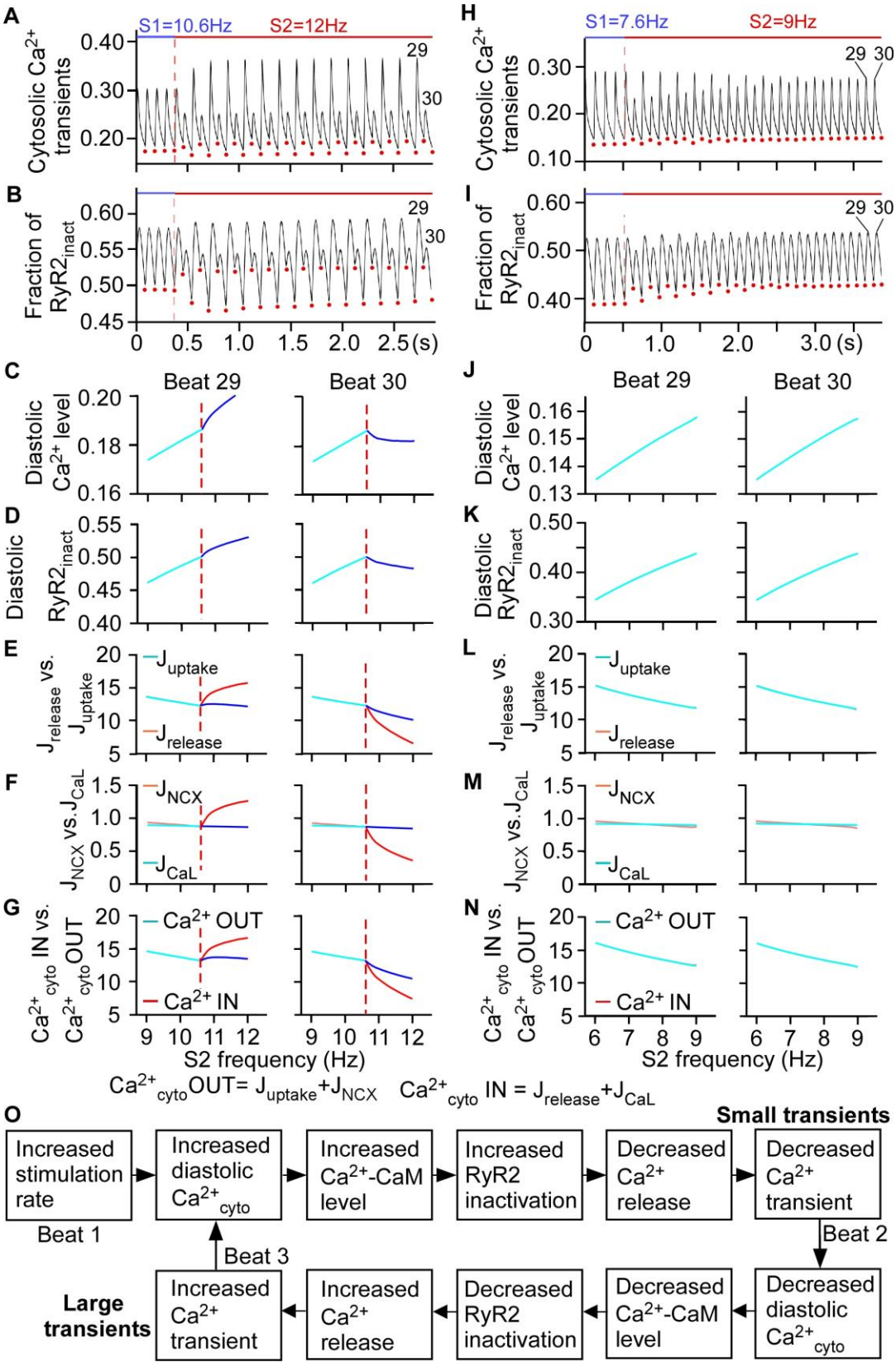
A
S1=10.6Hz
S2=12Hz
Cytosolic Ca2+ transients
29
30
B
Fraction of RyR2inact
C
Beat 29
Beat 30
Diastolic Ca2+ level
D
Diastolic RyR2inact
E
Jrelease vs. Juptake
Juptake
Jrelease
F
JNCX vs.JCaL
JNCX
JCaL
G
Ca2+cyto IN vs. Ca2+cyto OUT
Ca2+ OUT
Ca2+ IN
S2 frequency (Hz)
H
S1=7.6Hz
S2=9Hz
I
J
K
L
M
N
Ca2+cyto OUT= Juptake+JNCX Ca2+cyto IN = Jrelease+JCaL
O
Small transients
Increased stimulation rate
Beat 1
Increased diastolic Ca2+cyto
Increased Ca2+-CaM level
Increased RyR2 inactivation
Decreased Ca2+ release
Decreased Ca2+ transient
Beat 2
Decreased diastolic Ca2+cyto
Decreased Ca2+-CaM level
Decreased RyR2 inactivation
Increased Ca2+ release
Increased Ca2+ transient
Beat 3
Large transients

Figure 8. Pacing-induced elevation of diastolic cytosolic Ca^{2+} causes RyR2 inactivation, Ca^{2+} flux imbalance, and Ca^{2+} alternans

We performed S1-S2 protocols with a S1 frequency at 10.6 Hz, just below the onset of alternans, and with S2 frequencies ranging from 9 to 12 Hz. An example is shown with S2 = 12 Hz, where alternans develop in both the cytosolic Ca^{2+} transient (**A**) and the fraction of inactivated RyR2 (**B**). We then measured, at each beat after the change in frequency, the diastolic values of cytosolic Ca^{2+} (**C**) and the diastolic fraction of inactivated RyR2 (**D**). For clarity, we indicate with red dots in (**A**) and (**B**) the diastolic points where these values are taken. We then measured the fluxes corresponding to each beat and integrate the currents over the duration of the beat, corresponding to fluxes across the SR by SR Ca^{2+} release (Jrelease) or uptake (J_{uptake}) (**E**), across the cell membrane by the L-type Ca^{2+} channel (I_{CaL}) and the Na/Ca^{2+} exchanger (I_{NCX}) (**F**), and the total Ca^{2+} in or out of the cytosol, as the sum of the previous fluxes (**G**). We also performed S1-S2 protocols with a S1 frequency at 7.6 Hz and S2 frequencies ranging from 6 to 9 Hz (below the alternans threshold frequency). Similarly, we analyzed cytosolic Ca^{2+} transient (**H**), the fraction of inactivated RyR2 (**I**), the diastolic cytosolic Ca^{2+} (**J**), the diastolic fraction of inactivated RyR2 (**K**), the SR Ca^{2+} release (Jrelease) and uptake (J_{uptake}) (**L**), the L-type Ca^{2+} channel (I_{CaL}) and the Na/Ca^{2+} exchanger currents (I_{NCX}) (**M**), and the total Ca^{2+} in or out of the cytosol (**N**). (**O**) Proposed mechanism for fast pacing-induced Ca^{2+} alternans.

SUPPLEMENTARY MATERIALS

Supplementary Methods

Animal studies

All animal studies were approved by the Institutional Animal Care and Use Committee at the University of Calgary and performed in accordance with the NIH guidelines. The RyR2-E4872Q and RyR2-R4496C knock-in mutant mice were generated as previously described [47, 65]. Adult RyR2-R4496C$^{+/-}$ and RyR2-E4872Q$^{+/-}$ heterozygous mutant and wildtype control mice (8-16 weeks) were used for all experiments. All animal experiments involved in adenovirus-mediated gene delivery in vivo were performed blindly to genotype and the type of adenoviruses. However, experiments with control animals (i.e. without adenovirus injection) were not blinded as they do not have scars resulted from surgery and injection. Animals were assigned randomly to the experimental groups, and both male and female animals were utilized in experiments. No animals were excluded from analyses. A minimum sample size (n = 6 per group) for animal studies was estimated using the G*Power3.1 program with an effect size of 2, a significant level (alpha) of 0.05, and power of 0.8. The effect size was estimated from a pilot study that compared the means in the Ca^{2+} alternans ratio between two control hearts and two mutant hearts. Sample sizes and p values can be found in figures and figure legends.

In vivo gene delivery and confocal Ca^{2+} imaging

In order to determine the impact of altered CaM function on Ca^{2+} alternans in cardiac cells in intact working hearts, replication-deficient adenoviruses expressing CaM-WT, CaM (1-4) or CaM-M37Q mutant or adenoviruses co-expressing CaM-WT/GFP or CaM (1-4)/GFP was directly injected into the anterior wall of the left ventricle using the method described previously [39]. The *in vivo* adenovirus infection of cardiomyocytes was accomplished via a single localized injection on the anterior wall, while the posterior wall was unaffected. Five days after adenovirus injection the hearts were isolated and Ca^{2+} transients in an area ~1-2 mm away from the injection site were measured in Langendorff-perfused intact hearts using confocal Ca^{2+} imaging [40, 41]. In addition to measuring Ca^{2+} transients in the adenoviral-infected anterior wall, we also measured Ca^{2+} transients from the non-infected posterior wall of the left ventricle to serve as an internal control.

Determination of recovery of Ca^{2+} transients

The recovery of voltage-induced Ca^{2+} transients was determined by using the S1S2 stimulation protocol as described previously with some modifications [16, 27, 28]. Briefly, Ca^{2+} transients in Rhod-2 AM loaded hearts were first induced at 5 Hz for 5 seconds (S1), followed by a single S2 stimulation at a specific interval. The hearts were repeatedly stimulated by a series of S1S2 protocols with progressively decreased S1S2 intervals (from 200 ms to 40 ms). Ca^{2+} transients before and after S2 stimulation were continuously recorded by using the Nikon-A1R confocal microscope in the line-scan mode.

Laser scanning confocal Ca^{2+} imaging of intact hearts

RyR2 WT and mutant mouse hearts were loaded with 4.4 μM Rhod-2 AM (Biotium, Inc. Hayward, CA) in oxygenated Tyrode's buffer (118 mM NaCl, 5.4 mM KCl, 25 mM $NaHCO_3$, 1 mM $MgCl_2$, 0.42 mM NaH_2PO_4, 11.1 mM glucose, 10 mM taurine, 5 mM creatine, and 1.8 mM $CaCl_2$, pH 7.4) via retrograde Langendorff perfusion system at 25°C for 45 minutes, as described previously [40, 41]. The Langendorff-

perfused hearts were placed in a recording chamber mounted onto the Nikon A1R microscope for *in situ* confocal imaging (line-scan) of Ca^{2+} signals from epicardial ventricular myocytes. The temperature of the heart was kept at 35°C throughout the experiment with 5 μM blebbistatin (Toronto Research Chemicals, Toronto, ON) to prevent motion artifact. The pixel size of the resulting line-scan images ranged between 1.8 ms and 2 ms in the temporal dimension and between 0.1 microns to 0.4 microns in the spatial dimension. Ca^{2+} alternans in the WT and mutant hearts was induced by rapid electrical stimulation at increasing frequencies (5-15 Hz, 6 V).

Isolation of ventricular myocytes

Mouse hearts were mounted on the Langendorff apparatus and perfused with warm (37 ℃) Krebs-Ringers-HEPES (KRH) buffer KRH (125 mM NaCl, 5 mM KCl, 1.2 mM KH_2PO_4, 6 mM glucose, 1.2 mM $MgCl_2$ and 25 mM Hepes, pH 7.4) for 3 min to get rid of the blood. The KRH buffer was then switched to digestion buffer containing collagenase type II (Worthington Biochem.) and protease (Sigma). The heart was perfused for 7~10 min until it became soft. Bovine serum albumin (BSA) was added to the buffer to stop digestion. The atria and other non-cardiac tissues were removed with scissors and discarded. The cells were suspended by gently pipetting until most of the cells were separated. The cell solution was transferred after filtering (through 200 μm mesh size) into a 50 ml tube, and was centrifuged at 1,000 g for 1 min. Supernatant was removed, and the pellet was re-suspended in 5 ml of resuspension solution containing 50 nM Ca^{2+}, and was allowed to sediment down for 7 min. This process was repeated 4 times. The final cell pellet was re-suspended in resuspension solutions with increasing Ca^{2+} concentration (100 nM, 250 nM, 500 nM and 1 mM). Cells were kept in solution containing 1 mM Ca^{2+} at room temperature (23 ℃) until use.

Single cell Ca^{2+} imaging of isolated ventricular myocyte

Mouse ventricular myocytes were isolated using retrograde aortic perfusion as described previously [65]. Isolated cells were kept at room temperature (23 ℃) in Krebs-Ringers-HEPES (KRH) buffer (125 mM NaCl, 12.5 mM KCl, 25 mM HEPES, 6 mM glucose, and 1.2 mM MgCl2, pH 7.4) containing 20 mM taurine, 20 mM 2,3-butanedione monoxime (BDM), 5 mg/ml albumin, and 1 mM free Ca^{2+} until use. Freshly isolated mouse ventricular myocytes were added to glass coverslips pre-coated with 50 μg/ml laminin, and loaded with 5 μM Rhod-2, AM (Molecular Probes, USA) in KRH buffer containing 1 mM Ca^{2+} for 20 min at room temperature. The glass coverslip pre-mounted to a recording chamber was then placed onto an inverted microscope (Nikon ECLIPSE Ti) equipped with a Nikon CFI Plan Apo VC 60xWI objective. Rhod-2 AM loaded cells were perfused with KRH buffer containing 2 mM extracellular Ca^{2+} and 5 μM blebbistatin at room temperature. The cells were paced by field stimulation using the S88X electrical stimulator (Grass, USA). Confocal line-scanning (512 pixels and 1.9 ms per line) were performed along the longitudinal axis of cells using the Nikon A1R confocal system. The recovery of Ca^{2+} transients was determined by using the S1S2 stimulation protocol. Ca^{2+} transients in Rhod-2 AM loaded cells were first induced at 1 Hz for 5 seconds (S1), followed by a single S2 stimulation at a specific interval. The cells were repeatedly stimulated by a series of S1S2 protocols with progressively decreased S1S2 intervals (from 1000 ms to 100 ms). Ca^{2+} transients before and after S2 stimulation were continuously recorded by using the Nikon-A1R confocal microscope in the line-scan mode. SR Ca^{2+} content was determined after steady state stimulation at 1 Hz for 10 seconds by measuring the amplitude of Ca^{2+} release induced by local delivery of 20 mM caffeine.

Whole cell patch-clamp recording of isolated ventricular myocytes

Mouse ventricular myocytes were isolated from 2-4 months old WT mice infected with adenoviruses co-expressing CaM-WT/GFP or CaM (1-4)/GFP. Ventricular myocytes were planted on cover glasses and perfused with recording bath solution containing (in mM) NaCl 137, CsCl 5.4, $MgCl_2$ 1, $CaCl_2$ 1.2, HEPES 10, Glucose 10, 4-Aminopyridine (4-AP) 2, pH 7.4 adjusted with NaOH. The intracellular recording pipette solution contains (in mM) CsCl 120, TEA-Cl 20, $MgCl_2$1, MgATP 5, Na_2GTP 0.2, HEPES 10, and EGTA 0.01, pH adjusted to 7.2 with CsOH. GFP-expressing cells were identified based on their green fluorescence. After obtaining whole cell voltage-clamp with a gigaohm seal, whole cell membrane capacitance was calculated as the time integral of the capacitive response to a 10mV hyperpolarizing step. Cells with significant leak current (≥100 pA) were rejected (≈40%). When measuring whole cell L-type Ca^{2+} currents (depolarized every 10 s), a series of resistances and membrane capacitances were compensated electronically (≥75%). All recordings were performed at room temperature (23 ℃). The recovery from inactivation of the L-type Ca^{2+} current in isolated ventricular myocytes was determined by using whole-cell patch-clamp recordings and the S1-S2 stimulation protocol as described previously [38, 42] with some modifications. Briefly, for each sweep in the S1-S2 pacing protocol, the cells first received a S1 pacing, followed by a single S2 stimulation with the S1-S2 interval (when the cell was repolarized to -80 mV) ranging from 20 ms to 400 ms, in a 20 ms step. The interval between each sweep was 10 s. For the S1 pacing, cells were paced at 1 Hz for 5 seconds. For each stimulus, the cells were depolarized to 0 mV from a holding potential of -80 mV for 500 ms. For S2 stimulation, the cells were depolarized to 0 mV from -80 mV for 500 ms.

Western blotting

Heart tissues around the adenovirus injection site on the anterior wall of the left ventricle were collected and frozen in liquid nitrogen. Frozen tissues were homogenized in 6 volumes of homogenizing buffer containing 30 mM KH_2PO_4, 5 mM EDTA, 40 mM NaF, 300 mM sucrose, and a protease inhibitor mixture (1 mM benzamidine, 4 μM leupeptin, 0.5 mM DTT, and 100 mM PMSF). Heart homogenates were solubilized in a solubilizing buffer containing 50 mM Tris-HCl (pH 7.5), 3% SDS for 1 hour at room temperature, and then incubated at 55 °C for 10 min. Tissue lysates were obtained by centrifuging at 14,000 rpm for 10 min at 4 °C to remove insolubilized materials. The protein concentration was determined using a BioRad protein assay kit. 40 μg of proteins were subjected to 15% SDS-PAGE and transferred onto nitrocellulose membranes at 100 V for 1 h at 4 °C. The nitrocellulose membranes containing the transferred proteins were blocked with 5% non-fat dry milk in PBS for 60 min. The blocked membrane was incubated with anti-calmodulin antibody (Abcam, ab124742, 1:5000 dilution) or anti-GAPDH antibody (Sigma, G9545, 1:5000) at 4 °C overnight, and then incubated with secondary anti-rabbit IgG (heavy and light) antibodies conjugated to horseradish peroxidase (Invitrogen, 31460, 1:20,000 dilution). After washing for 10 min three times, the bound antibodies were detected using an enhanced chemiluminescence kit (Pierce). Images were taken and analyzed using the ImageQuant LAS 4000 (GE Healthcare/Life Sciences).

Image and signal processing

The signal and image processing methods were implemented using MATLAB (The Mathworks Inc., Boston, MA) as previously described [27]. Briefly, line-scan fluorescence images were filtered according to the noise level estimated by the median absolute deviation of the pixel intensities. Individual cells in the images were manually marked and the average fluorescence in each cell obtained for further analysis. A wavelet peak detection algorithm was used in order to detect individual Ca^{2+} release events in the average fluorescence signals. For each event detected in each cell, we determined the peak amplitude (local min-max difference) and the alternans ratio (relative amplitude difference between

consecutive peaks). The presence of alternans periods was established when six consecutive peaks presented an alternans ratio above 0.05. Alternans duration was defined as the percentage of alternans periods over the total line-scan duration. Average magnitudes were obtained by taking the mean over each line-scan. Alternans ratio increases with increasing pacing frequency, and the alternans threshold frequency at different experimental conditions was defined as alternans ratios >15%.

Statistical Analysis

All data shown are mean ± s.e.m, unless indicated otherwise. For assessing the normality of distribution of data, Shapiro-Wilk test was performed. For normally distributed data sets, parametric tests were performed. For non-normally distributed data sets, non-parametric methods were used. For non-parametric analyses, Mann-Whitney *U* test (two-sided) was used for two groups; Kruskal-Wallis test with Dunn's post hoc test was used for 3 or more than 3 groups. For parametric analyses, Student's *t*-test (two-sided) was used for two groups; One-way or two-way ANOVA followed by either Dunnett's or Bonferroni's post hoc test was used for 3 or more than 3 groups. Factorial designs were analyzed with two-way ANOVA test followed by Dunnett's post-hoc test. Although multiple comparisons in some experiments (alternans ratios at different frequencies and recovery at different S1S2 intervals) were carried out and analyzed systematically, no experiment-wide multiple test correction was performed. For isolated cardiomyocyte data, analyses were performed in RStudio using the hierarchical statistical method described previously by Sikkel et al. [64]. Statistical analyses were performed with GraphPad Prism 8 (GraphPad Software, CA) or Origin Pro 8.5 software (Origin Pro 8.5, Origin Lab Corporation, Northampton, MA, USA). Sample sizes and P values can be found in figure legends and/or figures. P values smaller than 0.05 were considered statistically significant.

Numerical modeling

Overview

Simulations are performed using a modified Bondarenko model [43] of a mouse ventricular myocyte. In order to assess the effects of CaM and RyR2 mutations on Ca^{2+} alternans, important modifications to the original Bondarenko model were made (Suppl. Fig. 4). The original model does not include RyR2 inactivation by the Ca^{2+}-CaM complex or by Ca^{2+} itself. Rather, inactivation is driven by the I_{CaL} current. Thus, we substituted the original RyR2 model by a four-state model [49], with a close, an open, and two inactivated states. We also added RyR2 inactivation by the Ca^{2+} -CaM complex as well as a steep dependence of the RyR2 open probability on SR luminal Ca^{2+}. Moreover, contrary to the original model, we do not assume instant binding of Ca^{2+} to CaM. Besides, in order to have a better correspondence with the experimentally measured quantities, we included mitochondrial and cytosolic Ca^{2+} dynamics and binding to the fluorescent dye Rhod-2 in our new model. All details of the new model can be found in the Supplementary Materials and modifications of the model can be found in Supplementary Tables 1-4.

Different CaM and RyR2 mutations were modeled using the following modifications: (1) CaM (1-4): decreased amount of available CaM, (2) CaM-M37Q: reduced the dissociation of Ca^{2+} from CaM [44], (3) RyR2-E4872Q: decreased opening rate of RyR2, increased close rate, slower recovery from inactivation, less cooperativity in the luminal Ca^{2+} activation of RyR2, larger I_{CaL} current, and increased Na^{+}/Ca^{2+} exchanger [47], (4) RyR2-R4496C: increased opening rate of RyR2 and higher cooperativity of the luminal Ca^{2+} [48, 66].

Detailed description of the model

We have adopted the Bondarenko model [43] of mouse ventricular myocytes with some modifications as described below. This model describes cellular electrical activity using an equivalent electrical circuit with subcellular compartmental spaces. It is assumed that there are no electrical gradients within the cell itself, i.e., the membrane potential is spatially homogeneous and all subcellular compartments are uniform or "well stirred".

The evolution of the transmembrane potential is given by the following equation:

$$-C_m \frac{dV}{dt} = I_{CaL} + I_{p(Ca)} + I_{NaCa} + I_{Cab} + I_{Na} + I_{Nab} + I_{NaK} + I_{Kto,f} + I_{Kto,s} + I_{K1} + I_{Ks} + I_{Kur} + I_{Kss} + I_{Kr} + I_{Cl,Ca} + I_{stim}$$

with the currents acting in different compartments, as indicated in the following schematic diagram from Bondarenko et al.[43].

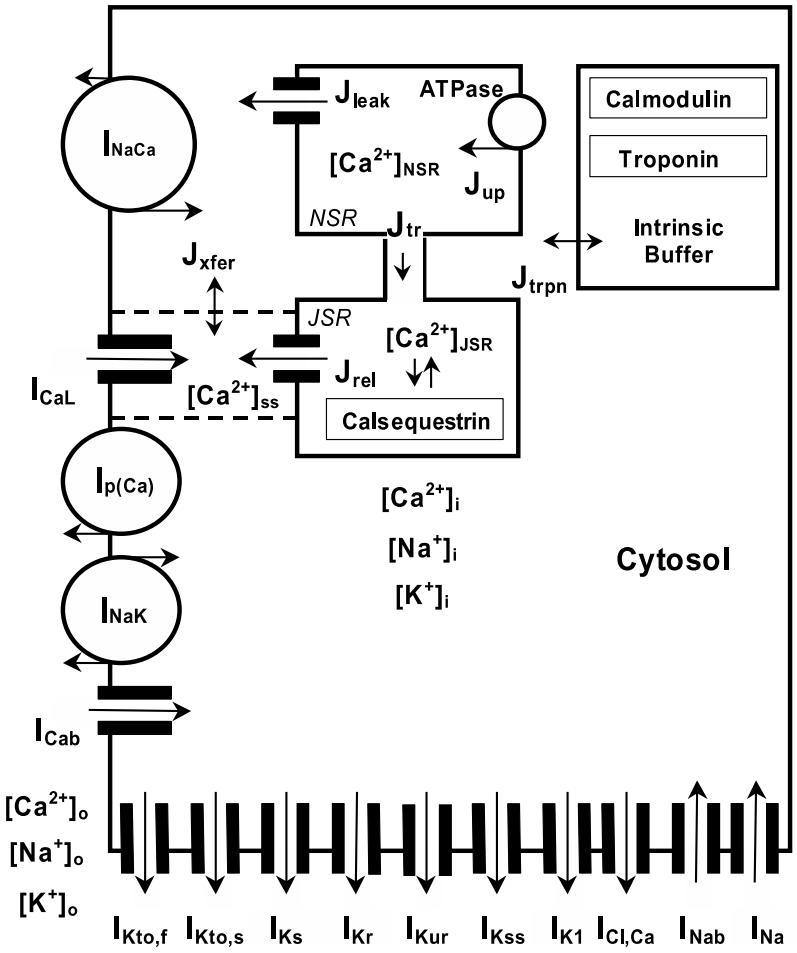

In this equation, V is the transmembrane potential, C_m is membrane capacitance, I_{Na} is the fast Na^+ current, I_{CaL} is the L-type Ca^{2+} current, $I_{Kto,f}$ is the rapidly recovering transient outward K^+ current, $I_{Kto,s}$ is the slowly recovering transient outward K^+ current, I_{Kr} is the rapid delayed rectifier K^+ current (mERG), I_{Kur} is the ultra-rapidly activating delayed rectifier K^+ current, I_{Kss} is the non-inactivating steady-state voltage-activated K^+ current, I_{K1} is the time-independent inwardly rectifying K^+ current, I_{Ks}

is the slow delayed rectifier K^+ current, I_{NaCa} is the Na^+/Ca^{2+} exchange current, $I_{p(Ca)}$ is the Ca^{2+} pump current, I_{NaK} is the Na^+/K^+ pump current, $I_{Cl,Ca}$ is the Ca^{2+}-activated Cl^- current, I_{Cab} and I_{Nab} are the background Ca^{2+} and Na^+ currents, respectively, and I_{stim} is the externally applied stimulation current.

Ca^{2+} in the Bondarenko model is considered to be in four compartments:

The cytosol, with Ca^{2+} concentration, $[Ca^{2+}]_I$, varying according to:

$$\frac{d[Ca^{2+}]_i}{dt} = B_i \left\{ J_{leak} + J_{xfer} - J_{up} - J_{trpn} - (I_{Cab} - 2I_{NaCa} + I_{p(Ca)}) \frac{A_{cap} C_m}{2V_{myo} F} \right\}$$

where I_{Cab}, I_{NaCa} and $I_{p(Ca)}$ are transmembrane currents, J_{leak} is a leak current from the SR, J_{xfer} is due to Ca^{2+} diffusion from the subsarcolemmal space, J_{up} is the current due to SERCA and J_{trpn} takes into account the binding and unbinding with troponim.

The subarcolemmal space, with concentration $[Ca^{2+}]_{ss}$, and time variation according to

$$\frac{d[Ca^{2+}]_{ss}}{dt} = B_{ss} \left\{ J_{rel} \frac{V_{JSR}}{V_{ss}} - J_{xfer} \frac{V_{myo}}{V_{ss}} - I_{CaL} \frac{A_{cap} C_m}{2V_{ss} F} \right\}$$

where J_{rel} is the release current from the SR, I_{CaL} is the L-type Ca^{2+} current, $J_{xfer\ is}$ the diffusive current between the subsarcolemmal and cytosolic spaces, V_{JSR}, V_{ss}, V_{myo} are the volumes of the junctional SR, subsarcolemmal and cytosolic spaces, and F Faraday's constant.

In the former two equations B_i and B_{ss} appear due to the instantaneous buffering to CaM, and are given by:

$$B_i = \left\{ 1 + \frac{[CMDN]_{tot} K_m^{CMDN}}{(K_m^{CMDN} + [Ca^{2+}]_i)^2} \right\}^{-1}, \quad B_{ss} = \left\{ 1 + \frac{[CMDN]_{tot} K_m^{CMDN}}{(K_m^{CMDN} + [Ca^{2+}]_{ss})^2} \right\}^{-1}$$

where $[CMDN]_{tot}$ it the total amount of CaM and K^{CMDN}_m the binding constant. In the Bondarenko model, these equations assume that Ca^{2+} binding to CaM is in equilibrium, i.e., instantaneous binding of Ca^{2+} to CaM.

The network SR space, with

$$\frac{d[Ca^{2+}]_{NSR}}{dt} = \left\{ J_{up} - J_{leak} \right\} \frac{V_{myo}}{V_{NSR}} - J_{tr} \frac{V_{JSR}}{V_{NSR}}$$

with J_{up} the current into the SR due to SERCA, J_{leak} a leak current from the SR into the cytosol, J_{tr} a diffusive current between the junctional and network SR spaces, V_{myo} the volume of the cytosol, and V_{NSR} and V_{JSR} the volumes of the network and junctional SR spaces.

The junctional SR space, with

$$\frac{d[Ca^{2+}]_{JSR}}{dt} = B_{JSR} \left\{ J_{tr} - J_{rel} \right\}$$

with J_{rel} the release current from the junctional SR into the cytosol. The term B_{JSR} is due to the binding to calsequestrin, that is also assumed to be instantaneous, so

$$B_{JSR} = \left\{ 1 + \frac{[CSQN]_{tot} K_m^{CSQN}}{(K_m^{CSQN} + [Ca^{2+}]_{JSR})^2} \right\}^{-1}$$

The constant $[CSQN]_{tot}$ is the total amount of calsequestrin and K^{CSQN}_m the binding constant of Ca^{2+} to CSQN.

The main modifications made to the model are the followings:

Dynamics of the buffers:

In our model we have introduced dynamics of binding and unbinding of Ca^{2+} to CaM. This is important to simulate some of the experimental conditions (gain-of-function CaM, with CaM-M37Q, see below) where these rates are modified. The binding of Ca^{2+} to CaM given by:

$$\frac{d[Ca\times CaM]}{dt} = k_{on}[Ca^{2+}]([CaM]_{tot} - [Ca\times CaM]) - k_{off}[Ca\times CaM]$$

with rates k_{on}=0.01ms^{-1}µM^{-1}, k_{off}=0.06ms^{-1}. From these, we obtain the binding constant K^{CMDN}_m=k_{off}/k_{on}=6 µM.

Besides, in order to compare with the experimental results, we have included dynamics of binding to the fluorescent dye Rhod-2.

Dynamics of the RyR2

In the original Bondarenko model, the release current from the SR is given by:

$$J_{rel} = \eta_1(P_{O_1} + P_{O_2})([Ca^{2+}]_{JSR} - [Ca^{2+}]_{ss})P_{RyR}$$

where v_1 is the conductance of the RyR2 channel, and the terms P_{O1} and P_{O2} are the fraction of RyR2 in two possible open states, according to the model of the RyR2 developed by Keizer & Levine [67] in the context of bullfrog sympathetic neurons, and adapted to cardiac myocytes by Jafri et al [68].

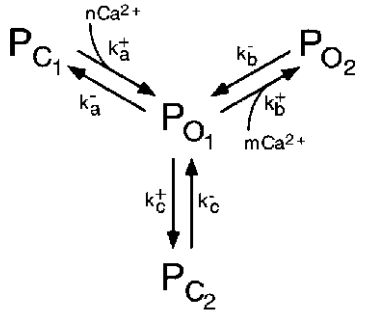

The term P_{RyR} is just a term introduced by the authors to obtain graded release. It is given by:

$$\frac{dP_{RyR}}{dt} = -0.04P_{RyR} - 0.1\frac{I_{CaL}}{I_{CaL,\max}}e^{\frac{-(V-50)^2}{648.0}}$$

This model of the RyR2 does not present inactivation per se. A type of inactivation is hidden in the dynamics of P_{RyR}, which needs some time to recover after Ca^{2+} entry from the extracellular space. However, inactivation is driven by the I_{CaL} current and not directly by Ca^{2+}. That is, a Ca^{2+} increase linked to I_{CaL} would produce inactivation, but a Ca^{2+} increase due to release from the SR would not. This may not be the case. Therefore, we have completely rewritten the SR release current and the dynamics of the ryanodine receptor gating. The release current is now in the form

$$J_{rel} = g_{rel} P_O([Ca^{2+}]_{JSR} - [Ca^{2+}]_{ss})$$

where g_{rel} is the conductance of the RyR2 channel, P_O its open probability, $[Ca^{2+}]_{JSR}$ the Ca^{2+} concentration at the junctional SR and $[Ca^{2+}]_{ss}$ the Ca^{2+} concentration at the subsarcolemmal (or dyadic) space. To calculate the RyR2 open probability we consider a four state model based on Stern et al [49] of the form

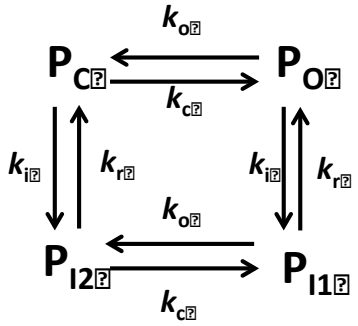

From the original model by Stern et al [49], we have introduced several modifications to include RyR2 inactivation by Ca^{2+} bound to CaM, luminal Ca^{2+} regulation of the RyR2 and the possibility of having alternans due to inactivation of the RyR2.

We assume that inactivation of the RyR2 (rate k_i) is not mediated by free Ca^{2+} but by Ca^{2+} bound to calmodulin, so

$$k_i = \tilde{k}_i [Ca \cdot CaM]$$

This is the main hypothesis of this work, which will be tested by comparison to the experimental results.

Activation of the RyR2 (rate k_o) is dependent on free Ca^{2+} at the dyadic space, and also on the junctional SR Ca^{2+} concentration. We thus introduce regulation of RyR2 by luminal Ca^{2+} [47, 69]. We assume that the open rate of the RyR depends on SR luminal Ca^{2+}, so the activation rate k_o is

$$k_o = \tilde{k}_o (1 + \alpha \xi(t)) [Ca^{2+}]_{ss}^2 \frac{[Ca^{2+}]_{JSR}^n}{K_{JSR}^n + [Ca^{2+}]_{JSR}^n}$$

The sigmoidal dependence on the junctional SR Ca^{2+} concentration, with an exponent typically of n=4-8, is what we call the booster. This agrees with the results by Shannon et al. [70], who found that the SR fractional Ca^{2+} release increased slowly and linearly with the increase in SR Ca^{2+} content (free $[Ca]_{SR}$ and total Ca^{2+}) but then rose very steeply when $[Ca]_{SR}$ exceeded a threshold concentration about 500μM.

We have included also a random variable $\xi(t)$ (distributed between -0.5 and 0.5), so the opening is not completely deterministic.

The rate of recovery from inactivation k_{im} is considered slow (of the order of 100-200 ms). This is necessary to obtain alternans due to a slow recovery of the RyR2 from inactivation [20, 30].

Effect of the mitochondria

In order to obtain a proper comparison with the experimental results, where Ca^{2+} is measured by levels of fluorescence, we have included the binding of Ca^{2+} to the Ca^{2+} indicator Rhod 2, both in the cytosol

and at the mitochondria. To do the latter, we have included a model for Ca^{2+} in the mitochondria as described previously [71]. The equation for Ca^{2+} in the mitochondria is given by:

$$\frac{d[\mathrm{Ca}^{2+}]_{\mathrm{m}}}{dt} = \delta(V_{\mathrm{uni}} - V_{\mathrm{NaCa}}),$$

where V_{uni} is the Ca^{2+} uniporter and V_{NaCa} the Na^{+}/Ca^{2+} exchanger across the mitochondrial membrane.

Simplification of Ca^{2+} extrusion

We have simplified Ca^{2+} extrusion from the cytosol, eliminating the I_{pCa} current and modifying the formulation of the NCX exchanger, now given by

$$I_{NaCa} = n_{NaCa} \frac{[Ca^{2+}]_{ss}^{nh}}{K_{mCa}^{nh} + [Ca^{2+}]_{ss}^{nh}} \frac{1}{K_m Na^3 + Na_o^3} \frac{1}{1 + k_{sat}\, e^{(h-1)za}} (e^{hza}\, Na_i^3 Ca_o - e^{(h-1)za}\, Na_o^3 [Ca^{2+}]_{ss})$$

with $za = V_m F / RT$

All the parameters corresponding to the previous modifications can be found in Supplementary Table 1.

Changes in parameters

As a result of the changes in the gating of the RyR2 with respect to the original model by Bondarenko et al. [43] the release current shape is slightly modified. Then, in order to reproduce the same calcium transients as in the original model, we had to fine tune also some of the parameters of the SERCA and LTCC functions (see Supplementary Table 2). We were especially careful to reproduce the increase in pre-systolic calcium load as the pacing frequency increases before the onset of alternans within the physiological range of frequencies.

Mutations

The different mutations are modeled by doing the following modifications in the model (Supplementary Table 3):

Gain-of-function CaM (CaM-M37Q): reduced dissociation of Ca^{2+} from CaM, i.e., decreased k_{off}. It should be noted that both overexpression of CaM-WT and CaM-M37Q would lead to an increase in the level of the CaM-WT and CaM-M37Q protein in relation to the level of endogenous CaM. Thus, to model the functional impact of overexpression of CaM-WT and CaM-M37Q, we increased the level of the total CaM for these cases, considering a level of total CaM that is the double of endogenous CaM. We also consider that a higher level of CaM increases the Ca^{2+}-dependent inactivation of the LTCC.

Loss-of-function CaM (CaM (1-4)): In the case of overexpression of the LOF CaM (1-4) mutation, the total CaM level is also increased. However, the CaM (1-4) protein is expected to bind to the same CaM binding site on the RyR2 as the endogenous CaM and hence prevent the binding and the effect of the endogenous CaM on RyR2 function. Thus, functionally, the effect of CaM (1-4) would be equivalent to a reduction in the total level of endogenous CaM, and in the model, we considered the effective CaM level in CaM(1-4) infected cells to be an half of the original value (i.e. the levels of endogenous CaM and CaM (1-4) are similar). Conversely, this also decreases the Ca^{2+}-dependent inactivation of the LTCC.

The mutants that modify RyR2 activity are modeled using parameters described in Supplementary Table 4.

Loss-of-function RyR2 E4872Q: decreased activity of the RyR2, decreasing the opening rate of the RyR2 (k_o), increasing the close rate (k_c), slower recovery from inactivation, less cooperativity in the luminal Ca^{2+} activation of RyR2 (booster), larger I_{CaL} current and increased Na^+/Ca^{2+} exchanger.

Gain-of-function RyR2-R4496C: increased activity of the RyR2, increasing the opening rate of the RyR2 (k_o) and the cooperativity of the booster (n) [48, 66].

Determination of alternans threshold frequency in the model

To determine the alternans threshold in the model, we paced it at different frequencies and measured the alternans amplitude (defined as the peak difference between two consecutive Ca^{2+} transients), as shown in the figure below. Among the modifications we did to the original Bondarenko model was the inclusion of a certain amount of stochasticity on the release to match what is observed in the experiments. That means that, close to the threshold of alternans, beat-to-beat alternations oscillate in amplitude with time. In Figs. 4 and 5 we thus show average values of the alternans ratio over a given (sufficiently large) time. A possibility to define the onset of alternans would have been to define a threshold amplitude for this ratio, as done in the experiments. Instead of doing that, that is somehow arbitrary, we have removed the stochasticity in the model, so we obtained a very well defined value of the frequency at which alternans appears, as can be observed in the figure below. This is how we have defined the threshold in the mathematical model.

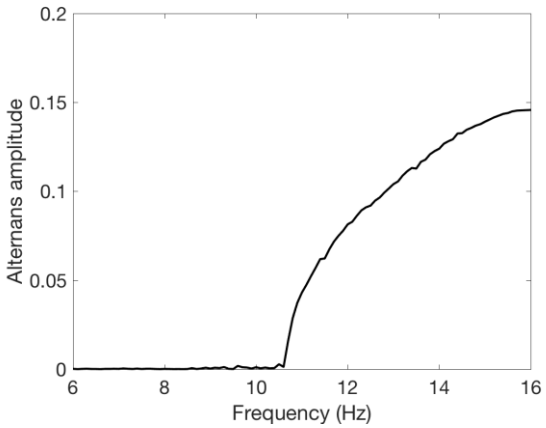

Onset of alternans as a function of frequency. Alternans amplitude (measured as the difference in cytosolic Ca^{2+} peak in two consecutive transients, in μM) as a function of pacing frequency. The amplitude is nearly zero up to a frequency of 10.6Hz, where it starts to grow, indicating the onset of alternans, in the form of a supercritical pitchfork bifurcation.

Supplementary Table 1: Parameters of the model.

Parameters of RyR2	Value	Units
Opening rate constant (k_o)	55/10000	$\mu M^{-2}\ ms^{-1}$
Half-Ca^{2+} luminal opening activation K_{jsr}	600	µM
Hill coefficient of luminal activation	6	-
Closing rate (k_c)	0.2	ms^{-1}
Inactivation rate constant (k_i)	15/10000	$\mu M^{-1}\ ms^{-1}$
Recovery from inactivation rate (k_r)	1/200	ms^{-1}
RyR2 conductance g_{rel}	1	ms^{-1}
Parameters Ca^{2+} Mitochondria		
Volume factor	0.3	-
Conductance mit. uniport (g_{uni})	5	ms^{-1}
Half-Ca^{2+}_{cyt} activation uniport K_a	0.2	µM
Reduction factor of the uniporter (L)	50	-
Hill coefficient uniporter	3	-
Maximum mit. NCX uptake (v^m_{ncx})	0.15	µM /ms
Half-Ca^{2+}_{cyt} activation NCX (K^c_{nx})	0.5	µM
Half-Na_{cyt} activation NCX (K^n_{nx})	10	mM
Parameters buffers		
Total amount of calmoudlin	22	µM
On rate of Ca^{2+}-CaM binding	0.01	$\mu M^{-1}\ ms^{-1}$
Off rate of Ca^{2+}-CaM binding	0.06	ms^{-1}
Total amount of Rhod2	20	µM
On rate of Ca^{2+}- Rhod-2 binding	0.1	$\mu M^{-1}\ ms^{-1}$
Off rate of Ca^{2+}- Rhod-2 binding	0.15	ms^{-1}
Total amount of SR binding sites	25	µM
Affinity	0.5	µM
Parameters NCX		
Maximum strength (ν_{NaCa})	2	A/(F µM)
Half-Ca^{2+}cyt activation (K_{mCa})	0.35	µM
Hill coefficient NCX activation	3	-

Supplementary Table 2: Modification in other parameters of the model

List of modified parameters	Orig	Mod.	Units
SERCA maximum uptake (ν_{up})	0.45	0.35	µM/ms
SERCA half-activation (K_{mup})	0.5	0.3	µM
Maximum LCC conductance (per unit capacitance g_{CaL})	0.17	0.15	mS/µF= ms^{-1}
Maximum time constant for Ca^{2+}-induced inactivation of LCC ($K_{pc,max}$)	233	52	s^{-1}
Half-saturation constant for Ca^{2+}-induced inactivation of LCC (Kpc,half)	20	6	µM

Supplementary Table 3: Parameters of the CaM mutants

Parameter	WT	WT(inj)	CaM(1-4)	CaM-M37Q
Total Amount Calmodulin (µM)	22	45	12	45
On rate of Ca^{2+}-CaM binding (μM^{-1} ms^{-1})	0.01	0.01	0.01	0.01
Off rate of Ca^{2+}-CaM binding (ms^{-1})	0.06	0.06	0.06	0.035
Maximum time constant for Ca^{2+}-induced inactivation of LCC (s^{-1})	52	68	48	68
Half-saturation constant for Ca^{2+}-induced inactivation of LCC (µM)	6	6	6	3.5

Supplementary Table 4: Parameters of the mutants that modify RyR2 activity

Parameter	WT	R4496C	E4872Q
Opening rate constant (μM^{-2} ms^{-1})	55/10000	60/10000	38/10000
Inactivation rate constant (μM^{-1} ms^{-1})	15/10000	25/10000	15/10000
Hill coefficient of luminal Ca^{2+} activation	6	7	4
Recovery from inactivation rate (ms^{-1})	1/200	1/125	1/260
Maximum LCC conductance (ms^{-1})	0.15	0.15	0.2
Maximum strength NCX (A/(F µM))	2	2	4

Unedited immunoblots

Fig. 2D

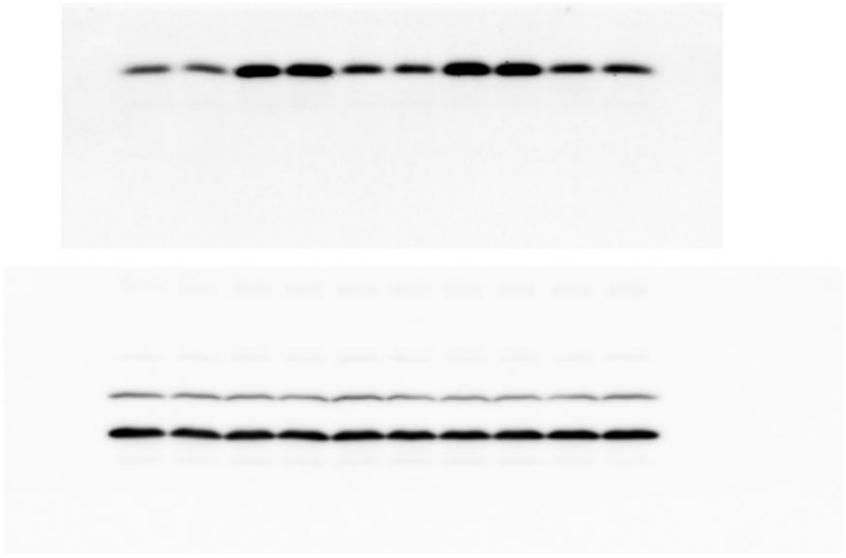

Supplementary Figure S1F

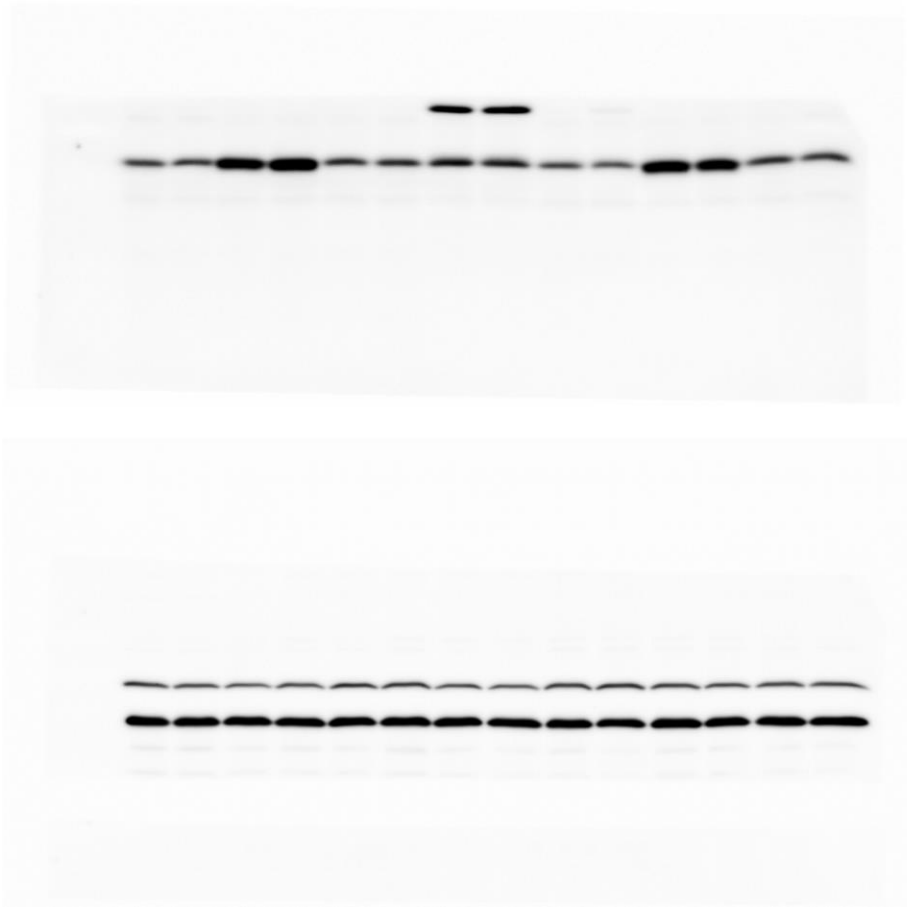

Supplementary Figures:

Figure S1

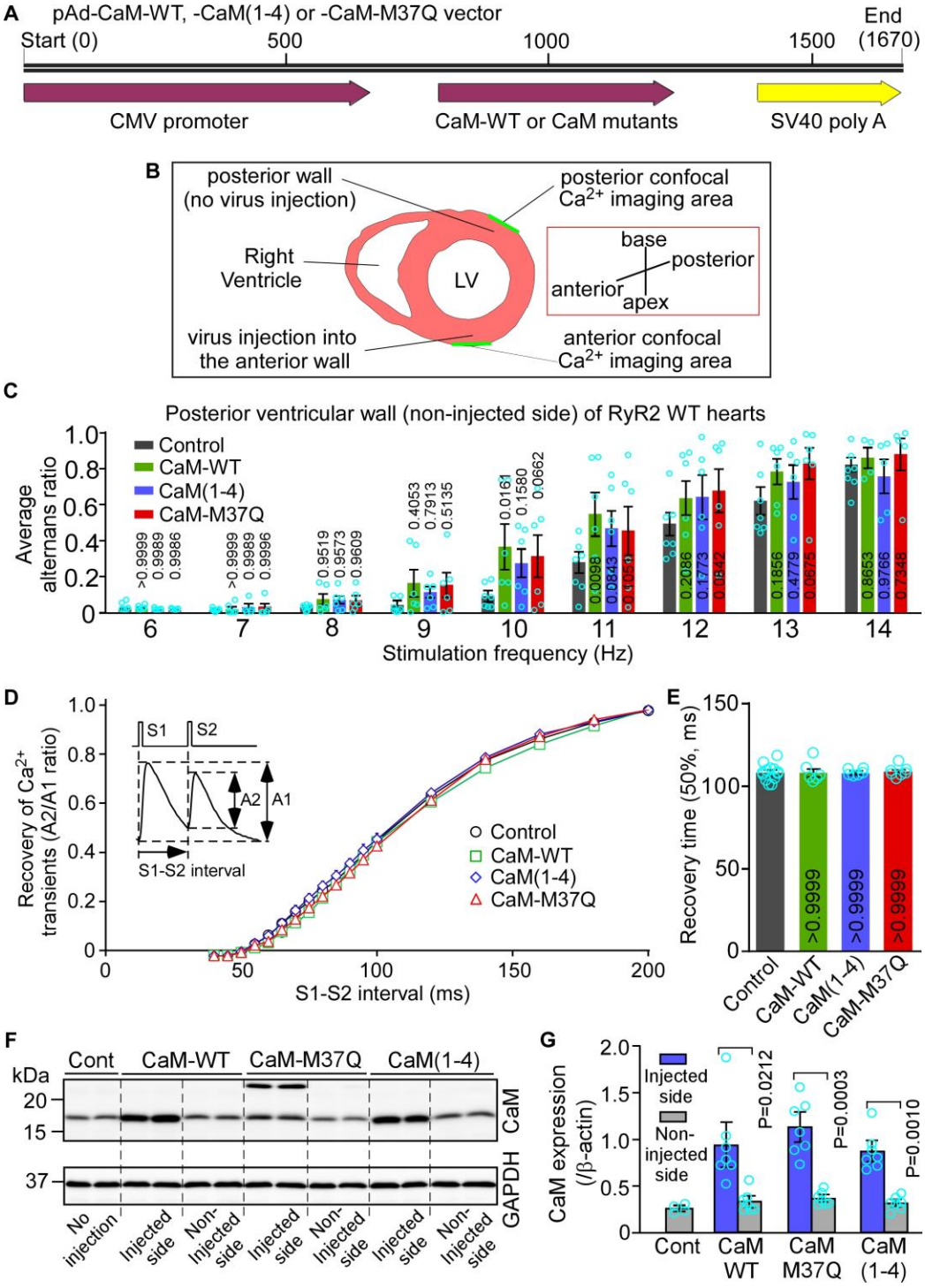

Supplementary Figure S1. Spatially limited impact and expression of locally injected CaM adenoviruses in intact RyR2 WT hearts

(**A**) A schematic diagram of plasmids used to produce the adeno-associated viruses (AAV) expressing CaM-WT, CaM(1-4), or CaM-M37Q. (**B**) A schematic diagram of in vivo local gene delivery through injection of CaM WT or CaM mutant adenoviruses into the anterior wall of the left ventricle and in situ imaging of Langendorff-perfused intact hearts. (**C**) Ca^{2+} transients in the posterior wall (away from the injection site) of the left ventricle of the intact Rhod-2 loade control or virus-injected hearts were recorded using line-scanning confocal imaging and analyzed to determine the average alternans ratios after pacing at increasing frequencies (6-14 Hz). Data are mean ± s.e.m. (n = 7 hearts for Control, 6 hearts for CaM-WT, 6 hearts for CaM (1-4), and 6 hearts for CaM-M37Q with their P values indicated for each condition vs control). (**D**) The recovery of Ca^{2+} transients and (**E**) the 50% recovery time of the Ca^{2+} transient amplitude after pacing with the S1S2 protocol. Data are mean ± s.e.m. (n = 13 hearts for Control, 6 hearts for CaM-WT, 6 hearts for CaM (1-4), and 7 hearts for CaM-M37Q with their P values indicated for each condition vs control). (**F**) Immunoblotting of tissues isolated from the anterior wall of the left ventricle of control hearts or from the left ventricular anterior wall around the sites of injection (injected sites) of CaM-WT, CaM-M37Q, or CaM (1-4) adenoviruses or from the posterior wall (away from the injection site, non-injected sites) of the left ventricle. (**G**) Quantification of CaM expression 5 days post adenoviral injection. Data are mean ± s.e.m. (n = 4 hearts for Control, 6 hearts for CaM-WT, 7 hearts for CaM (1-4), and 7 hearts for CaM-M37Q) with their P values indicated for each condition vs non-injected site) (Two-way ANOVA with Dunnett's post-hoc test for obtaining the adjusted p-values shown in (**C**, **D**) (all conditions vs control), Kruskal-Wallis test with Dunn's post-hoc test for obtaining the adjusted p-values shown in (**E**) (all conditions vs control), and paired Student's *t*-test, injected side vs non-injected site (**G**)).

Figure S2

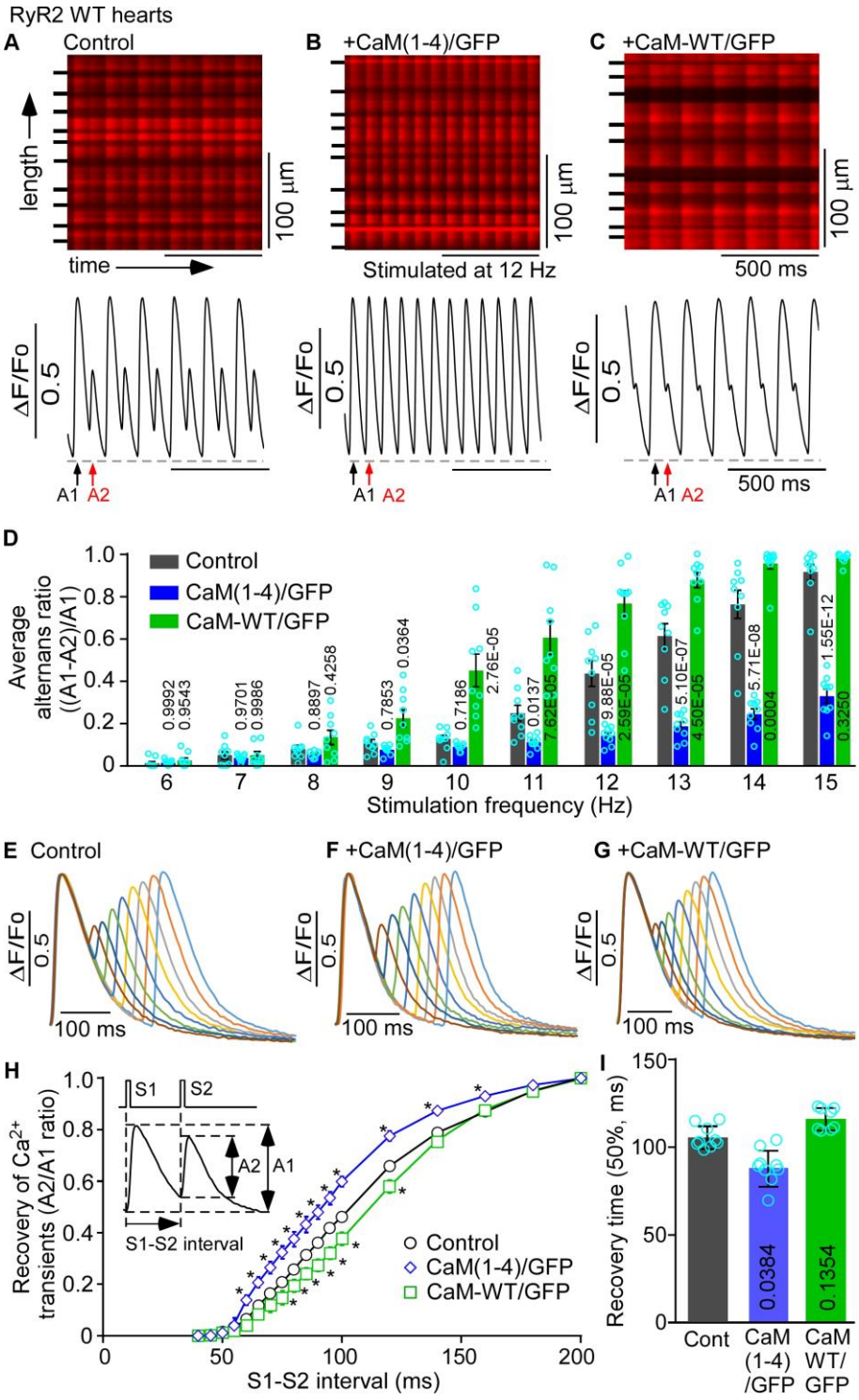

Supplementary Figure S2. Effects of CaM-WT/GFP and CaM (1-4)/GFP on Ca^{2+} alternans and Ca^{2+} transient recovery in intact RyR2 WT hearts.

RyR2-WT hearts without injection (**A**, Control) and with local injection of CaM (1-4)/GFP (**B**) or CaM-WT/GFP (**C**) adenoviruses were stimulated at increasing frequencies (6-15 Hz). (**D**) Alternans ratios.

Data are mean ± s.e.m. (n = 9 hearts for Control, 9 hearts for CaM (1-4)/GFP, and 9 hearts for CaM-WT/GFP with their P values indicated for each condition vs control). Recovery of Ca^{2+} transients in control (**E**), CaM (1-4)/GFP (**F**) or CaM-WT/GFP (**G**) hearts. (**H**) The relationship between A2/A1 ratio of the Ca^{2+} transient amplitude and the S1S2 interval (*p<0.05 vs control). (**I**) The 50% recovery time of the Ca^{2+} transient amplitude after pacing with the S1S2 protocol. Data are mean ± s.e.m. (n = 9 hearts for Control, 9 hearts for CaM (1-4)/GFP, and 8 hearts for CaM-WT/GFP with their P values indicated for each condition vs control) (Two-way ANOVA with Dunnett's post-hoc test for obtaining the adjusted p-values shown in (**D**, **H**), Kruskal-Wallis test with Dunn's post-hoc test for obtaining the adjusted p-values shown in (**I**), all conditions vs control).

Figure S3

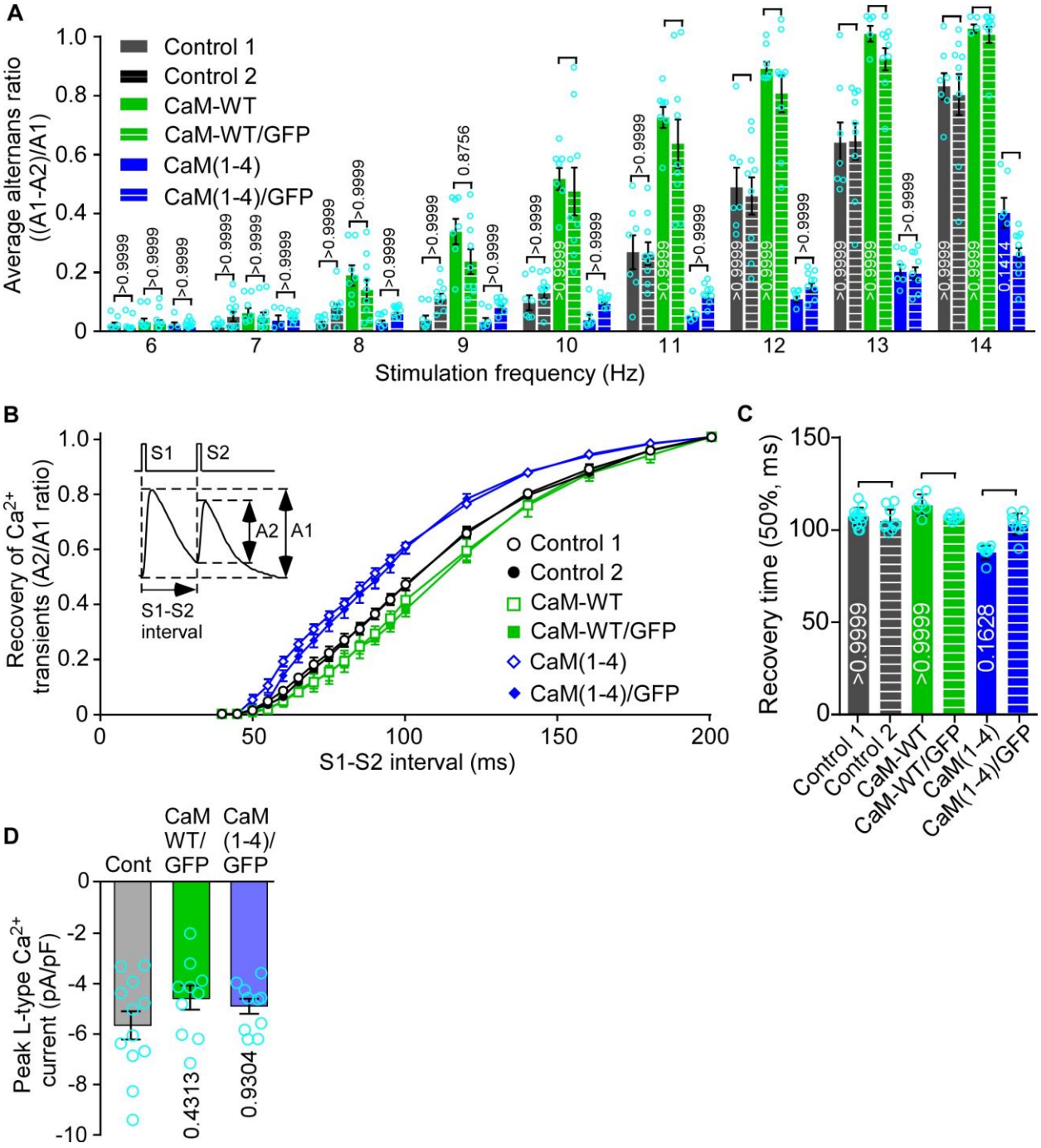

Supplementary Figure S3. Comparison of the impact between CaM-WT and CaM-WT/GFP and between CaM (1-4) and CaM (1-4)/GFP, and effects of CaM-WT/GFP and CaM (1-4)/GFP on the peak L-type Ca^{2+} current

(**A**) Alternans ratios in CaM-WT, CaM-WT/GFP, CaM (1-4) and CaM (1-4)/GFP adenovirus infected hearts stimulated at increasing frequencies (6-14 Hz). Data are mean ± s.e.m. (n = 7 hearts for Control 1, 9 hearts for Control 2, 6 hearts for CaM-WT, 8 hearts for CaM-WT/GFP, 6 hearts for CaM (1-4),

and 9 hearts for CaM (1-4)/GFP with their P values indicated for each comparison) (**B**) The relationship between A2/A1 ratio of the Ca^{2+} transient amplitude and the S1S2 interval. (**C**) The 50% recovery time of the Ca^{2+} transient amplitude after pacing with the S1S2 protocol. Data are mean ± s.e.m. (n = 13 hearts for Control 1, 9 hearts for Control 2, 6 hearts for CaM-WT, 8 hearts for CaM-WT/GFP, 8 hearts for CaM (1-4), and 9 hearts for CaM (1-4)/GFP with their P values indicated for each comparison). (**D**) The averaged peak L-type Ca^{2+} current densities in control, CaM-WT/GFP and CaM (1-4)/GFP adenovirus expressing cells. Data are mean ± s.e.m. (n = 12 cells from 6 hearts for Control, 10 cells from 5 hearts for CaM-WT, and 10 cells from 5 hearts for CaM (1-4) with their P values indicated for each condition vs control; Values of s.e.m. were adjusted with hierarchical statistical methods [64], One-way ANOVA with Bonferroni's post-hoc test for obtaining the adjusted p-values shown in (**D**) (Two-way ANOVA with Bonferroni's post-hoc test for obtaining the adjusted p-values shown in (**A**, **B**), Kruskal-Wallis test with Dunn's post-hoc test for obtaining the adjusted p-values shown in (**C**), all conditions vs control).

Figure S4

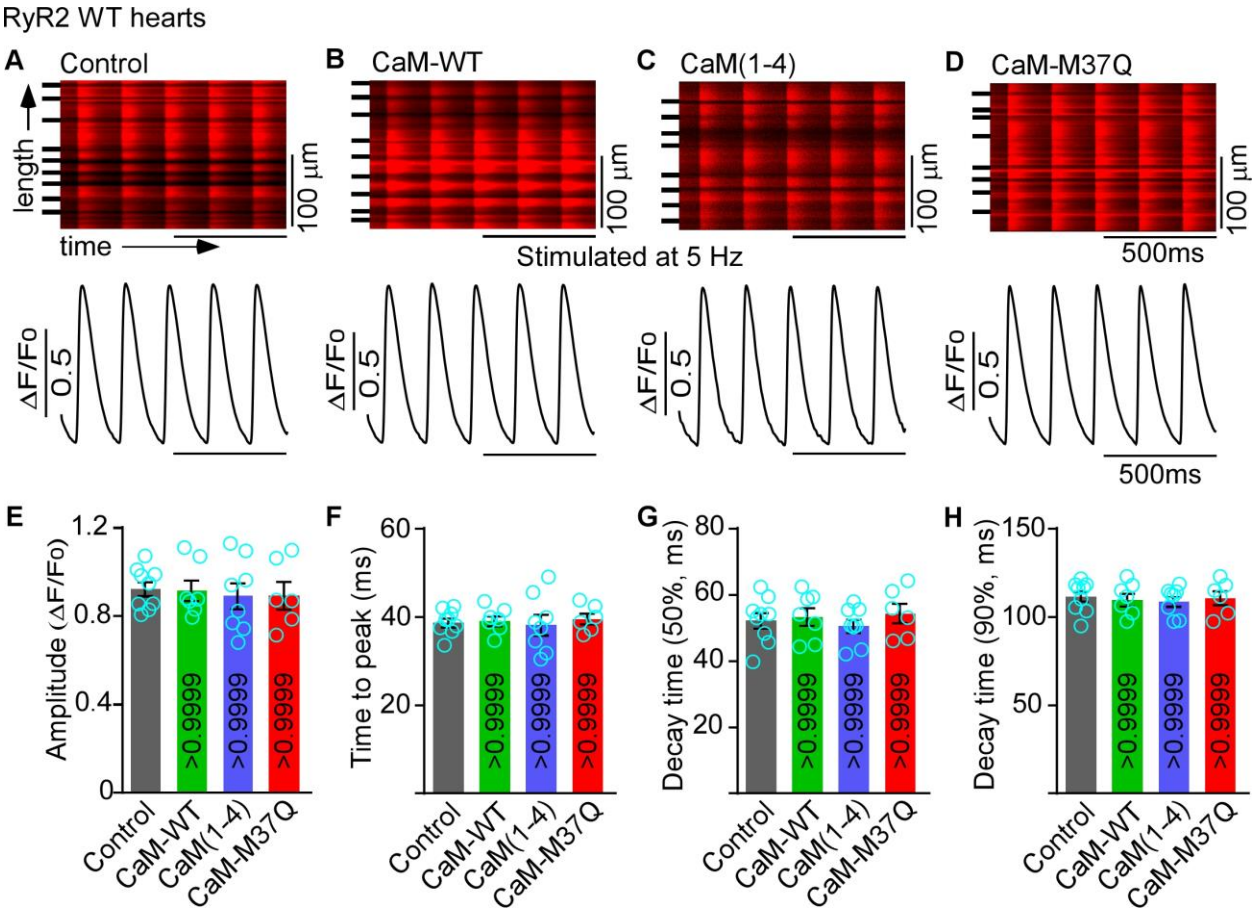

Supplementary Figure S4. Effects of altered CaM function on Ca^{2+} transient properties of intact RyR2 WT hearts

RyR2 WT hearts without injection (**A**, control) or locally injected with adenoviruses expressing CaM-WT (**B**), CaM (1-4) (**C**) or CaM-M37Q (**D**) were loaded with Rhod-2 AM. Ca^{2+} transients in intact Rhod-2 AM loaded hearts were elicited by pacing at 5 Hz and recorded using line-scanning confocal imaging. Cell boundaries were indicated by short bars to the left. The ΔF/Fo traces depict the average fluorescence signal of the scan area. (**E**) Amplitude, (**F**) time to peak, (**G**) time to 50% decay of Ca^{2+} transients, and (**H**) time to 90% decay of Ca^{2+} transients at 5 Hz. Data shown are mean ± s.e.m. (n = 9 hearts for Control, 7 hearts for CaM-WT, 8 hearts for CaM (1-4), and 6 hearts for CaM-M37Q with their P values indicated for each condition vs control) (Kruskal-Wallis test with Dunn's post-hoc test for obtaining the adjusted p-values shown in (**E-H**), all conditions vs control).

Figure S5

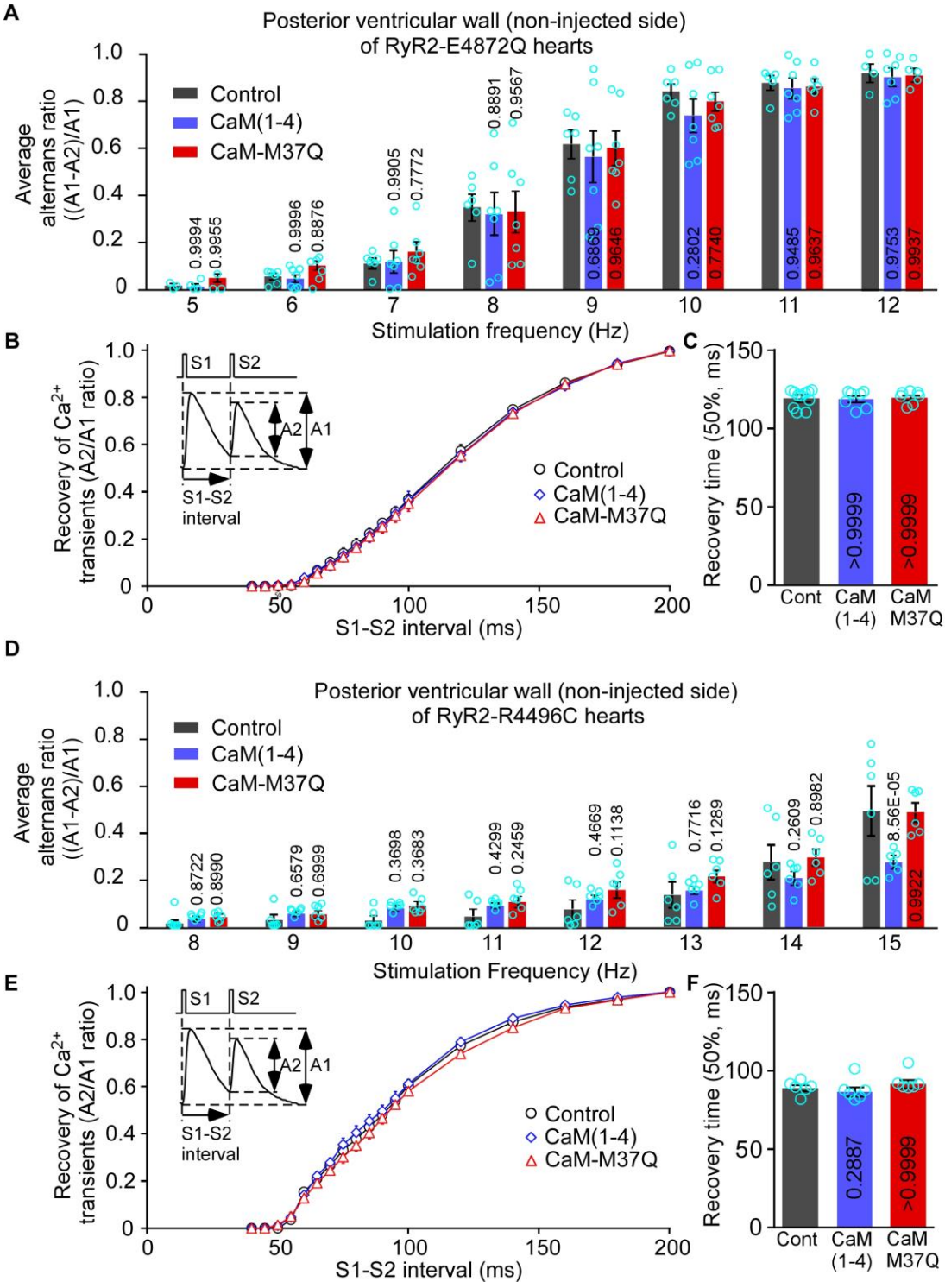

Supplementary Figure S5. Spatially limited impact of locally injected CaM adenoviruses in intact RyR2-E4872Q and RyR2-R4496C hearts

Langendorff-perfused intact RyR2-E4872Q or RyR2-R4496C hearts without injection (control) or locally injected with adenoviruses expressing CaM(1-4) or CaM-M37Q into the anterior wall of the left

ventricle were loaded with Rhod-2 AM. Ca^{2+} transients in the posterior wall (away from the injection site) of the left ventricle of the intact Rhod-2 loaded hearts were recorded using line-scanning confocal imaging. (**A**) The average alternans ratios after pacing at increasing frequencies (5-12 Hz) on RyR2-E4872Q hearts. Data are mean ± s.e.m. (n = 6 hearts for Control, 7 hearts for CaM (1-4), and 7 hearts for CaM-M37Q with their P values indicated for each condition vs control). (**B**) The relationship between A2/A1 ratio of the Ca^{2+} transient amplitude and the S1S2 interval on RyR2-E4872Q hearts. (**C**) The 50% recovery time of the Ca^{2+} transient amplitude after pacing with the S1S2 protocol on RyR2-E4872Q hearts. Data are mean ± s.e.m. (n = 11 hearts for Control, 7 hearts for CaM (1-4), and 7 hearts for CaM-M37Q with their P values indicated for each condition vs control). (**D**) The average alternans ratios after pacing at increasing frequencies (8-15 Hz) on RyR2-R4496C hearts. Data are mean ± s.e.m. (n = 6 hearts for Control, 6 hearts for CaM (1-4), and 6 hearts for CaM-M37Q with their P values indicated for each condition vs control). (**E**) The relationship between A2/A1 ratio of the Ca^{2+} transient amplitude and the S1S2 interval on RyR2-R4496C hearts. (**F**) The 50% recovery time of the Ca^{2+} transient amplitude after pacing with the S1S2 protocol on RyR2-R4496C hearts. Data are mean ± s.e.m. (n = 6 hearts for Control, 6 hearts for CaM (1-4), and 6 hearts for CaM-M37Q with their P values indicated for each condition vs control) (Two-way ANOVA with Dunnett's post-hoc test for obtaining the adjusted p-values shown in (**A**, **B**, **D**, **E**), Kruskal-Wallis test with Dunn's post-hoc test for obtaining the adjusted p-values shown in (**C**, **F**), all conditions vs control).

Figure S6

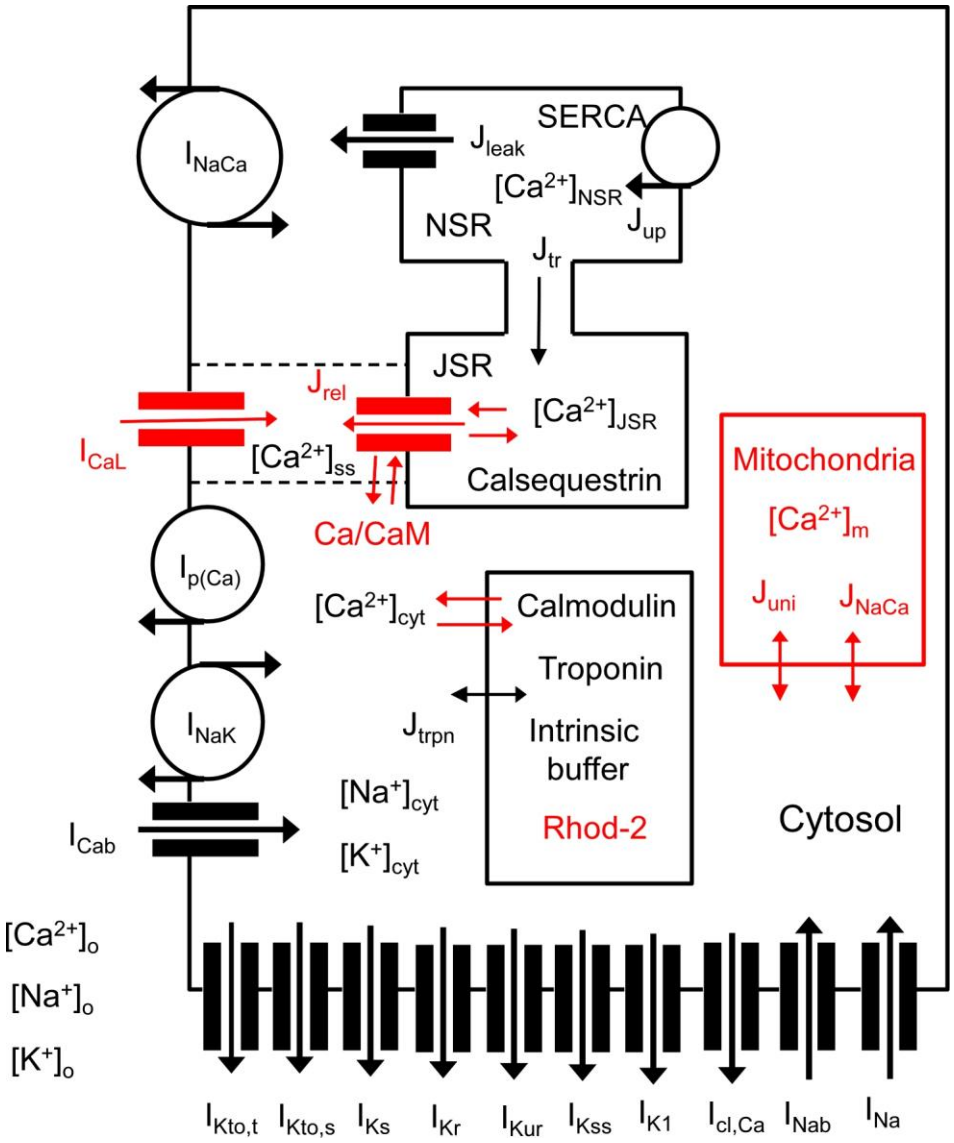

Supplementary Figure S6. Schematic illustration of the major components of the cardiac cell model for simulating Ca^{2+} alternans

Modified Bondarenko model with various compartments and currents. In red we show the modifications made in the current work. We have modified the form of the I_{CaL} and SR release currents. For the former, we have considered that its Ca^{2+}-dependent inactivation depends on the level of CaM. For the latter, we have considered a four-state model of the RyR2 that incorporates activation by luminal Ca^{2+}, and inactivation by Ca^{2+} bound to CaM. Due to the importance of CaM we have incorporated its binding dynamics to Ca^{2+}, which was assumed to be in equilibrium in the original model. Besides, to get a better comparison with experiments, we have incorporated the fluorescent Ca^{2+} dye Rhod-2, and its binding to Ca^{2+}, as well as the dynamics of Ca^{2+} at the mitochondria, that also gives a contribution to the fluorescence signal.

Figure S7

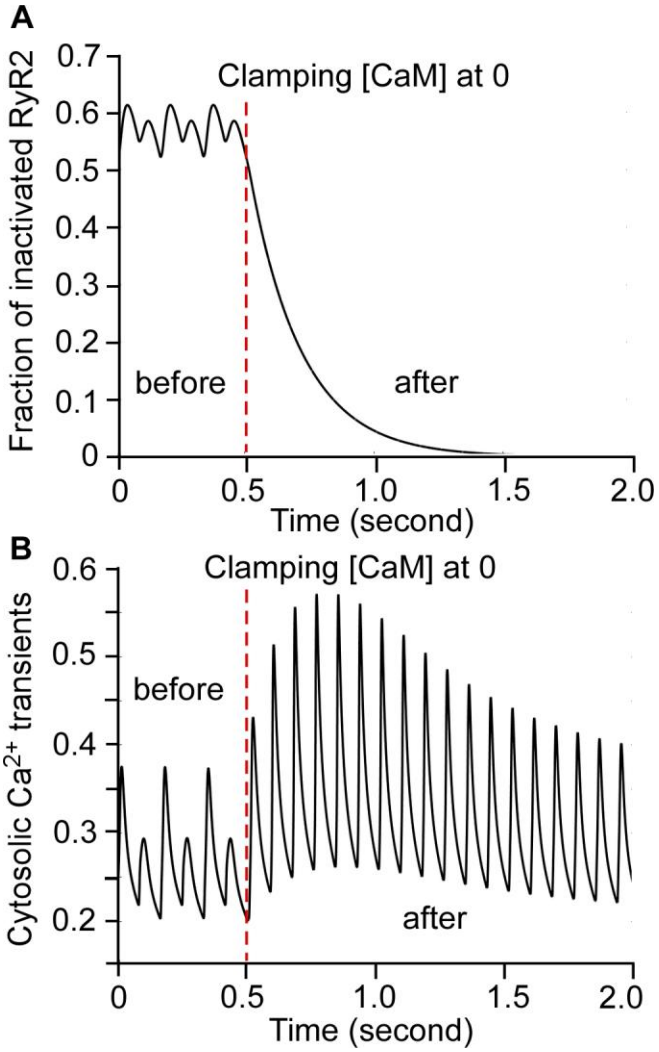

Supplementary Figure S7. Role of CaM in RyR2 inactivation and Ca^{2+} alternans

At a stimulation frequency of 12 Hz, the model presents sustained alternans. To assess the role of CaM, we set the concentration of CaM to zero (**A**). After this, the fraction of inactivated RyR2 decreases to zero, as they recover from the inactivated state, and cannot be inactivated again. This lack of inactivation results in an instant removal of alternans (**B**).